A Method to Reduce the Effects of Plasma Contamination and First Wall Erosion in Fusion Reactors

G.L. Kulcinski, R.W. Conn, G. Lang,
L. Wittenberg, D. Sze, J. Kesner, D.L. Kummer

August 9, 1974
(revised September 15, 1974)

UWFDM-108

FUSION TECHNOLOGY INSTITUTE

UNIVERSITY OF WISCONSIN

MADISON WISCONSIN

A Method to Reduce the Effects of Plasma Contamination and First Wall Erosion in Fusion Reactors

G.L. Kulcinski, R.W. Conn, G. Lang, L. Wittenberg, D. Sze, J. Kesner, D.L. Kummer

Fusion Technology Institute
University of Wisconsin
1500 Engineering Drive
Madison, WI 53706

http://fti.neep.wisc.edu

August 9, 1974 (revised September 15, 1974)

UWFDM-108

A Method to Reduce the Effects of Plasma Contamination and First Wall Erosion in Fusion Reactors

by

Gerald L. Kulcinski
Robert W. Conn
G. Lang[a]
L. Wittenberg[b]
D. Sze
J. Kesner
D. L. Kummer[a]

Nuclear Engineering Department
University of Wisconsin
Madison, Wisconsin

UWFDM-108

August 9, 1974
Revised September 15, 1974

(a) McDonnell-Douglas Astronautics Co.-East
(b) Monsanto Research Corporation

I. Introduction

II. Properties of Graphite Cloth

III. Specific Considerations for the Graphite Curtain

- A. Deployment of curtain
- B. Material specifications
- C. Vacuum pump-down
- D. Temperature consideration
  1. Equilibrium curtain temperature
  2. Thickness of stand-off pads required
  3. Time behavior
- E. Mechanical Properties
- F. Neutronic Properties
- G. Displacement damage and swelling
- H. Sputtering of graphite curtain
- I. Effect on tritium inventory
- J. Compatibility
- K. Electrical effects
- L. Miscellaneous

IV. Plasma Effects

- A. High Z vs Low Z Impurities - Impact on Energy Balance
- B. Impact in Tokamaks
- C. Estimated Impurity Levels in a Plasma
- D. Other Plasma Effects

V. Conclusions

I. Introduction

Considerable concern has been expressed recently about the erosion of metallic vacuum walls by charged particles leaking from tokamak plasmas[1] and the resulting plasma contamination effects of these metallic impurities.[2] High Z impurities have the most significant effect on plasma performance since they will not be fully stripped of all electrons. This is true of materials such as Mo, Nb, and W and the resulting line and recombination radiation can be orders of magnitude larger than bremsstrahlung.[3] Even for Fe, which will probably be fully stripped at plasma temperatures above 10 keV, recombination radiation is still larger than bremsstrahlung. The result is that the plasma $n\tau$ required to obtain ignition is substantially increased.[4,5] For tokamaks, this means the plasma current required to achieve ignition will be considerably higher than required for a pure D-T plasma.[5] On the other hand, low Z impurities have a much less serious impact on plasma performance and larger concentrations of such materials can be tolerated.

The object of this paper is to describe a mechanism by which the benefits of low Z first walls can be achieved while at the same time taking advantage of the high strength and ductility of a metallic vacuum wall which is not damaged by wall erosion.

The basic problem is that the ions of a reactor grade plasma (deuterium, tritium, and helium) as well as 14.1 MeV neutrons will be incident on the first wall facing the plasma. Some of the atoms on the first wall will be ejected back into the plasma chamber causing wall erosion as well as plasma contamination. The impact of such impurities in the plasma is twofold. First, as noted already, impurity atoms with high Z will cause increased energy

losses via line, recombination and bremsstrahlung radiation. Second, in a β-limited plasma (β is the ratio of plasma pressure to magnetic field pressure) the total plasma pressure is limited. At fixed β, an increase in impurity ions causes a decrease in the density of hydrogenic ions since

$$n_e = n_i + 2n_\alpha + Z_{im}\, n_{im}$$

Here, Z_{im} is the charge on the impurity and n_e, n_i, n_α, n_{im} are the electron, hydrogenic ion, alpha and impurity densities, respectively. Since the fusion power is proportional to n_i^2, a reduction in n_i has a large effect on the total power output. The alpha heating rate of the plasma is also dependent on n_i and will be decreased if impurities enter the plasma. These facts coupled with the increased radiative losses, will cause a further degradation of plasma performance. For example, a self-sustaining plasma can be transformed into an unignited system as the impurity atom density increases. Alternatively, if impurity atoms are present before the plasma is heated, they can cause a significant increase in the temperature required for ignition. This means that, for tokamak systems a large increase in plasma current is required to achieve ignition conditions.[5] Low Z impurities considerably reduce these general effects.

On the other side of the problem, the removal of wall atoms can occur by several mechanisms; sputtering by neutrons, deuterium, tritium and helium , "particle" emission by 14 MeV neutrons and blistering by charged particle (D^+,T^+,He^{++}) bombardment.[6] Various mechanisms such as divertors and gas blankets have been proposed to reduce the wall erosion due to charged particles but there is no known mechanism to reduce the neutron sputtering. However, even with divertors, which may be ~90% effective, the wall fluxes are quite high, e.g. $\sim 10^{14}$ particles/cm^2/sec for D&T and

$\sim 10^{13}$ particles/cm^{2}sec of helium.[8] The neutron fluxes are $\sim 10^{14}$ n/cm^2/sec.

The problem is then, how can we reduce the plasma contamination rate and at the same time protect the first wall from known and well established erosion mechanisms? The first approach might be to make the wall out of a low Z material such as carbon or SiC. However, construction of massive structures which can withstand high tensile as well as compressive stresses over many cycles and still maintain vacuum tightness appears to be out of the question with present day technology.[7]

The next approach might be to coat metallic construction materials with low Z elements to protect them and the plasma. However, differential expansion, differential radiation induced swelling and differences in thermal conductivity make the adherence of such a coating extremely difficult. Chemical effects on potential CTR materials such as carburizing V or Nb, also must be carefully considered.

The method which we propose is to place a "carbon cloth curtain" between the plasma and first wall. (See Figure 1) This curtain will intercept all (>99.9%) of the photons and charged particles from the plasma thus protecting the metallic first wall. The curtain will be cooled only by radiation and therefore it will radiate the heat uniformly to wall, eliminating hot spots from inhomogeneous particle fluxes. The curtain will also prohibit any metallic atoms from reaching the plasma and it will keep any neutron induced chunks from entering the plasma.

The graphite itself will suffer radiation damage (to be covered later) and carbon atoms will be sputtered (and perhaps blistered) from the curtain surface into the plasma. However, since the atomic number of carbon is only 6,

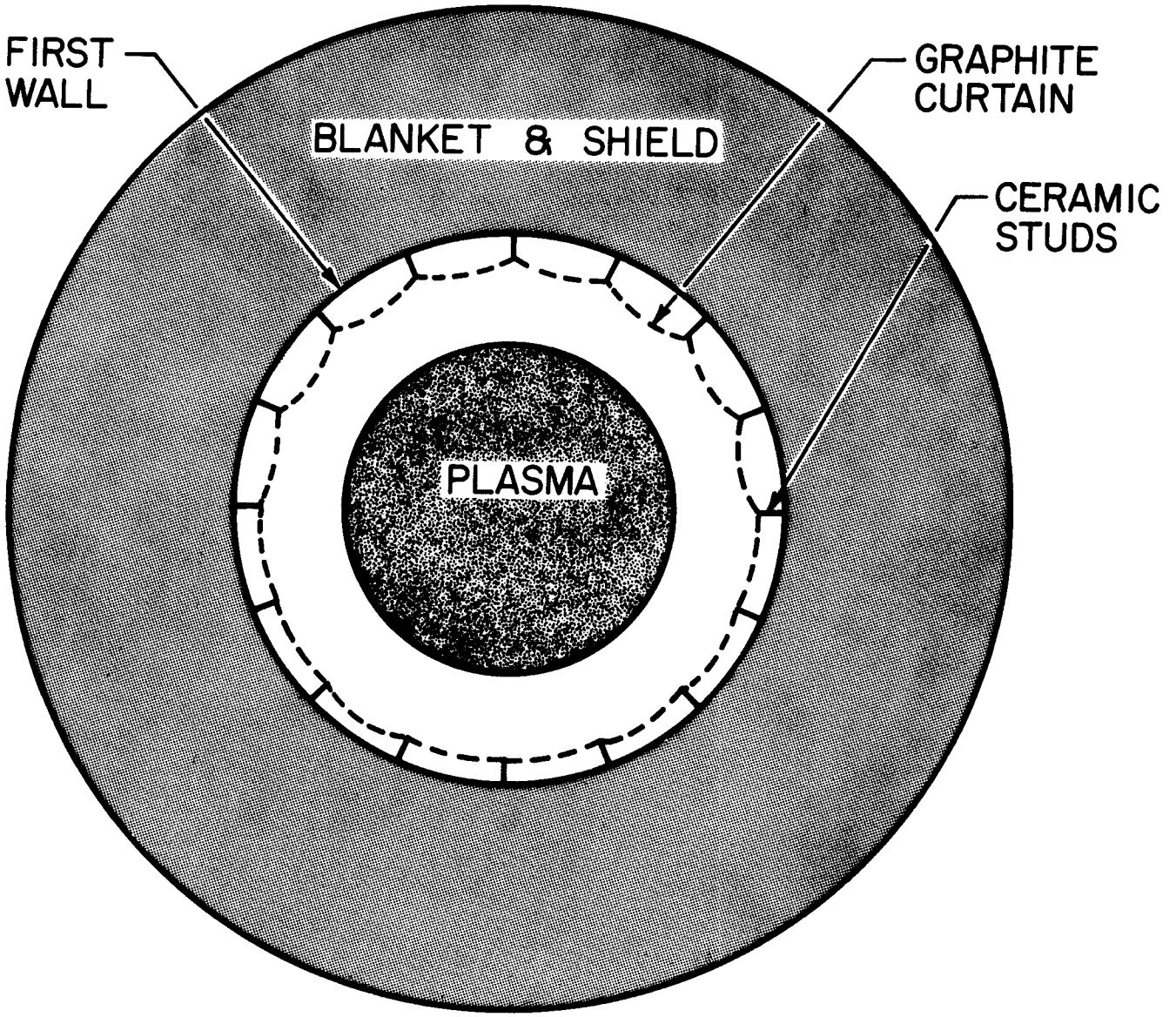

Figure 1. Placement of carbon curtain between plasma and fusion reactor first wall to reduce the effects of plasma contamination and reduce first was erosion.

the contamination effects will be far less than for the corresponding number of metallic atoms as we have seen previously.

The remainder of this report will contain a brief description of the properties of graphite cloth, and a point by point preliminary investigation of this concept. In order to obtain more quantitative numbers, we will use the reactor parameters of UWMAK-II[9] for subsequent calculations. It is worthwhile to list at this time, the advantages and disadvantages of this particular concept (see Table I).

Table I

Features of the "Carbon Curtain" Approach

Potential Advantages	Potential Disadvantages
Low Z_{eff}	High Internal Helium Generation
Low Self Sputtering Coefficient	Radiation Growth
Low Neutron Activation	
No Special Cooling Required (Radiation Sufficient)	
Intercepts All Ions and Neutral Atoms from Plasma	
Intercepts Metallic "Chunks" and High Z Atoms from First Wall	
No Structural Role (can also withstand limited failure)	
Reduces "Hot Spots" to First Wall Due to Inhomogeneous Particle Flux (both in normal operation and in failure mode)	
Reduces "Scrape Off" Region Around Plasma	
Reduces Tritium Inventory in First Wall Facing Plasma	
May Allow the Removal of Divertors on Tokamaks	
(Making TF coils smaller and placement of field magnets less critical)	
Absorbs Synchrotron Radiation	

II. Description and Properties of Fibrous Carbon and Graphite

A. Preparation

Fibrous carbon and graphite is prepared by the controlled thermal conversion of organic fibers to residual carbonaceous material. The precursor organic fibers must have a number of specific properties in order to produce an acceptable carbon fiber. They must decompose without a melt phase, they should pyrolyze without appreciable liberation of carbon containing gases in order to retain the carbon content of the original organic fiber and they should form a strong, yet flexible carbonaceous residue.

Initially, regenerated cellulose yarn or woven cloth (such as rayon) was used to obtain such products. Subsequently, the strength and modulus of these rayon based yarns were greatly increased by mechanically stretching the fibers during pyrolysis and then heating to graphitization temperatures. More recently polyacrylonitrile (PAN) yarn has been used as a precursor. With this fiber an initial oxidation treatment is performed on the fiber by heating in air at 200°-300°C while under tension.

The carbon fibers are produced by pyrolysis at relatively low temperatures, e.g. less than 1000°C. The graphite products receive an additional step in which the temperature is raised to 2000°C or more. The materials that are mechanically worked during pyrolysis are produced only as yarns which must be subsequently woven if fabric is desired.

The carbon or graphite yarns consist of bundles of 700-1000 continuous filaments varying from 6 to 10 microns in diameter. These bundles or tows may be used as is or they may be twisted to form a twisted yarn or thread. Any number of tows may be twisted together to form yarns of any diameter. Generally a coating or finish is applied to the yarn to protect it from abrasion during the weaving process. This finish may then be removed by a thermal treatment.

Most of the common textile techniques for producing fabrics can also be applied with varying success to the carbon and graphite yarns. These include filament winding, felting, knitting, braiding, weaving cloth and weaving thicker products in three dimensions by means of specialized looms. Different weave patterns such as the square weave, satin weave or twill weave have been applied to carbon or graphite cloth. The most commonly applied are the square weave and either a 5 harness or 8 harness satin weave. Figure 2 shows a graphite cloth in the square weave modification at successively higher magnifications. The openings between yarns can be reduced by changing the weaving procedures and the yarn geometry. However, total opacity for the graphite curtain application will likely require the use of 3 or more layers of fabric.

Weaving in three dimensions allows for an even greater number of variations. In Figure 3, two of these variations are schematically shown namely, the orthogonal weave in which the 3 yarns are at right angle to each other and the angle interlock pattern in which the "c" direction yarns are woven at an angle to the plane of the other 2 yarns. Additional construction details and properties of commercially available carbon and graphite are collected in Table 2.

An advantage of carbon and graphite in fibrous form is its flexibility. Both the structure and the small diameter of the individual filaments contribute to the pliant quality of these materials. This is in marked contrast to the characteristic brittleness of the standard forms of graphite.

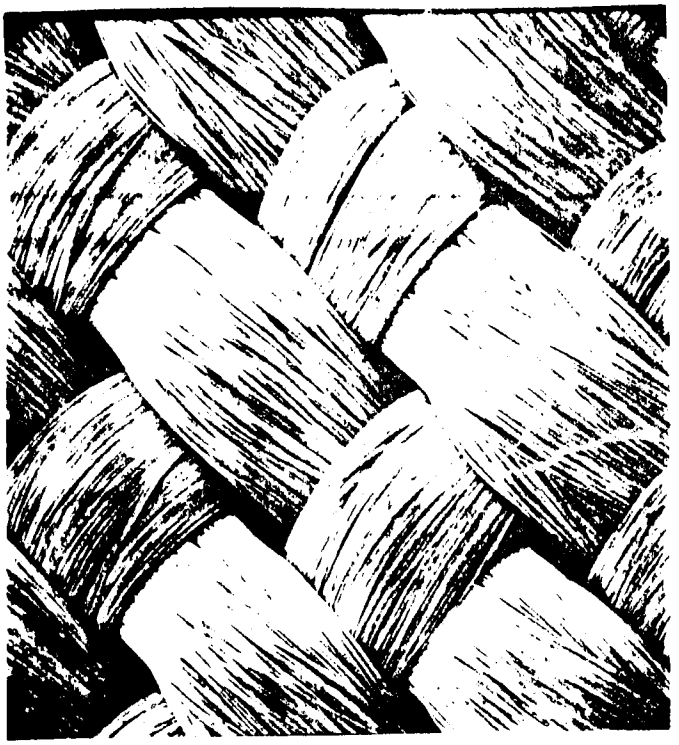

x25

x 100

x1000

x 5000

Figure 2. Photographs of Graphite Fabric at a Number of Magnifications

negative no.: 30982-C-2

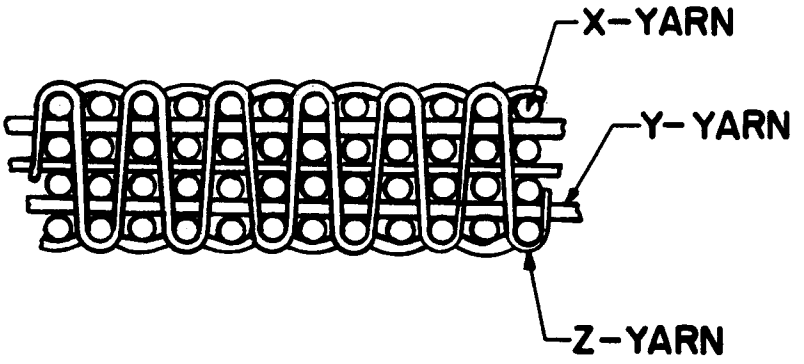

ORTHOGONAL WEAVE

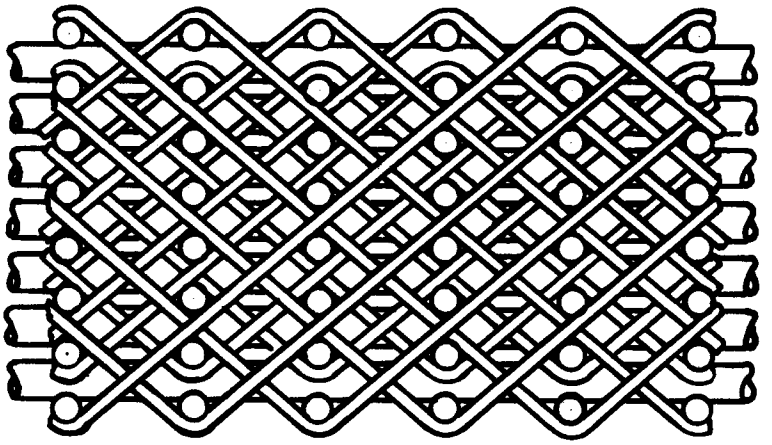

ANGLE INTERLOCK WEAVE

Table 2

Properties of Carbon and Graphite Fabric

Property	Carbon Fabrics	Graphite Fabrics
Weight, g/m^2	250-290	210-270
Thickness, cm	0.038-0.066	0.028-0.064
Count, yarns/cm		
Warp	11-20	11-21
Fill	9-19	9-18
Filaments/yarn	960-1600	960-1600
Porosity cm^3 voids/g	1.06-1.28	1.42-1.46
Permeability $cm^3/sec/cm^2$	60-71	58-61
Tensile Break Strength, kg/cm	1.8-3.0	6.8-8.9
Electrical Surface Resistance ohm/cm^2	11	0.06-0.08

B. Molecular Structure of Fibrous Carbon

When organic polymer fibers are carbonized the carbon residue retains some of the structure of the long chain organic polymers. At this point, however, the carbon is largely amorphous as determined by X-ray crystallography, and it may retain appreciable amounts of hydrogen, nitrogen, and oxygen. After being exposed to graphitization temperatures, the material takes on a distinctive graphite structure.

A proposed model of the crystal structure of PAN fibers (Reference 10) is shown in Figures 4-5. The basic structural unit (Figure 4) appears to be a ribbon-like graphite layer about 60Å in width and several thousand Å long. A number of these ribbons are stacked parallel to form a microfibril with a preferred orientation parallel to the fiber axis. The microfibrils are wrinkeled and contain many discontinuities so that long narrow voids (about 200-300 Å) occur at the boundaries of the microfibrils (Figure 5). These discontinuities will likely influence the effects of charged particles from the plasma impinging on the graphite curtain in that the resultant gas atoms may more readily escape.

C. Properties of Carbon and Graphite Yarn

1. Strength and Stiffness

The room temperature modulus of the carbonaceous fibers continually increases with increasing graphitizing temperature. The room temperature strength shows an initial increase, reaches a maximum and thereafter decreases. See Figure 6 (Reference 11). The exception is the unstretched rayon based fiber which does not increase in either strength or modulus when graphitized.

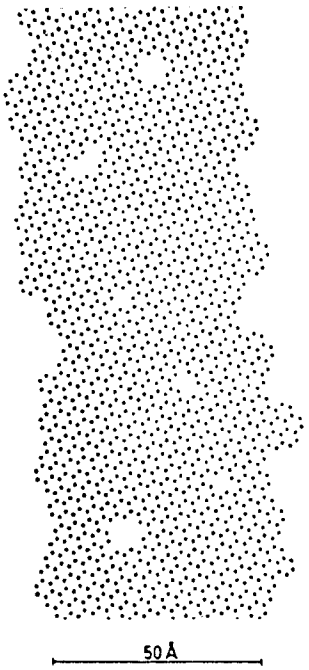

Figure 4 Schematic Representation of the Structure of a Ribbon

Figure 5 Schematic Representation of the Structure of Carbon Fibers

Using the strength and modulus as a criteria, the commercially available yarns may be divided into the five categories shown in Table 3a. These are:

a. Low modulus, low strength carbon.

b. Intermediate modulus, high strength carbon.

c. Low modulus, low strength graphite.

d. Intermediate modulus, intermediate strength graphite.

e. High modulus, intermediate strength graphite.

The highest strength, 425,000 psi, is obtained with the PAN based carbon fiber whereas the highest modulus 70-90 million psi is obtained with the most highly graphitized ray or PAN based fibers.

A unique property of carbon and graphite is its high temperature strength. Unlike most materials, it becomes stronger with temperature reaching a maximum strength at 2500°C which is approximately twice its room temperature strength. Above this temperature, the strength rapidly decreases. This relationship for graphite products is shown on a relative basis in Figure 7 (Reference 12).

2. Thermal Properties

Thermal conductivity in the axial direction varies by more than a factor of 5 between carbon fibers and the highly graphitized material. The carbon and low modulus graphite fibers have values in the 0.173-0.26 watt/cm/°C whereas the high modulus materials have values of 1.2 or more.

Thermal expansion in the axial direction decreases for materials that are more highly graphitized. The carbon fibers exhibits mean values from room temperature to 1500°C of around 1% while the graphitized materials have values of less than 0.2%. Indeed below 500°C graphite fibers have a negative coefficient of expansion as can be seen in Figure 8 which is the curve for Thornel-75, a fully graphitized rayon based fiber. (Reference 13) In the same diagram, the thermal expansion in the radial direction is shown to be

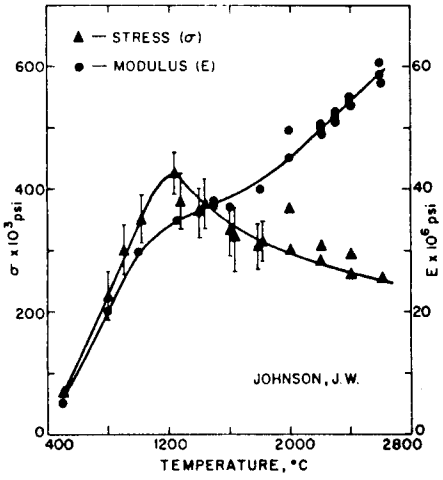

Figure 6 Room Temperature Strength and Modulus of Carbon Fibers as a Function of the Pyrolysis Temperature

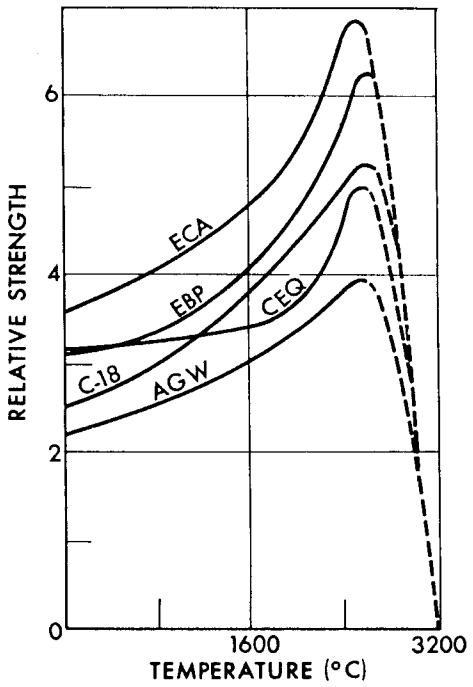

Figure 7 Relative Tensile Strength vs. Temperature for Various Graphites

Table 3a

Properties of Carbon and Graphite Yarn

	Low Modulus Low Strength	Intermediate Modulus High Strength	Low Modulus Low Strength	Intermediate Modulus Intermediate Strength	High Modulus Intermediate Strength	
Precursor	Rayon	PAN	Rayon	Rayon	Rayon	PAN
Modulus, Psi x 10^6	5-10	30-40	5-25	30-40	50-75	50-75
Ultimate Strain %,	1.5-3.0	1.0-1.3	1.6-2.1	.5	.5	.5
Tensile Strength, psix10^3	100-180	400-425	100-180	250-300	300-375	200-350
Fiber Density, g/cc	1.45-1.50	1.6-1.8	1.5-1.6	1.7-1.8	1.85	1.9-2.0
Carbon Assay, w/o	90-99	92	99.5	99.9	99.9	99.9
Thermal Conductivity	0.23	0.19-0.43	0.19-0.26	0.19-0.21	1.2-1.6	1.3
Axial Thermal Expansion Axial, % R.T.-1500°C	0.7-1.0	0.3-0.4	0.2-3	.25	.14	-
Specific Heat Cal/gr°C R.T.-150°C	0.22	0.22	0.22	0.22	0.22	0.22

considerably higher. This illustrates the anisotropic nature of these materials resulting from their unique crystal structure.

Vapor pressure of graphite is negligible up to 3000°C. Even under a high vacuum it is practical to use graphite up to 2000°C. Graphite vaporizes in a number of modes releasing molecules with 1, 2, 3 or more carbon atoms. The vapor pressure of these various species as a function temperature is shown in Figure 9a. (Reference 12) The vaporization rate of carbon is given in in Figure 9b and Table 3b.

3. Additional Property Considerations

One advantage to a material in fibrous form that should be noted is its versatility. By varying the fiber composition, the type of yarn, the type of weave geometry some peoperties can be varied over a relatively large range. In addition, fibrous materials other than graphite may be woven into the forms to further change the properties. Within limits, the material can be tailored to fit a wide range of requirements.

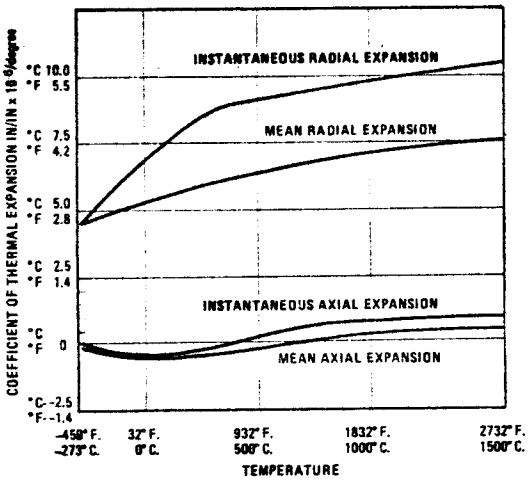

Figure 8 Coefficient of Thermal Expansion of Graphite Fibers vs. Temperature

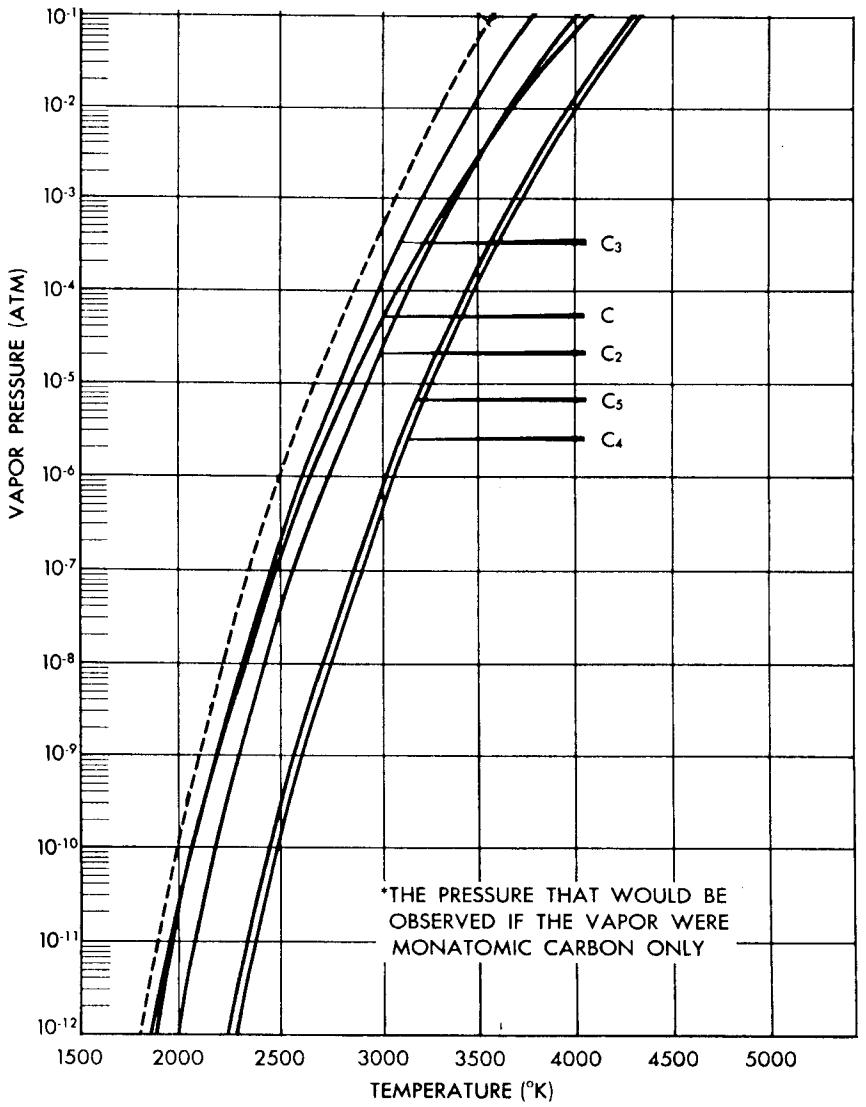

Figure 9a Vapor Pressure of Graphite

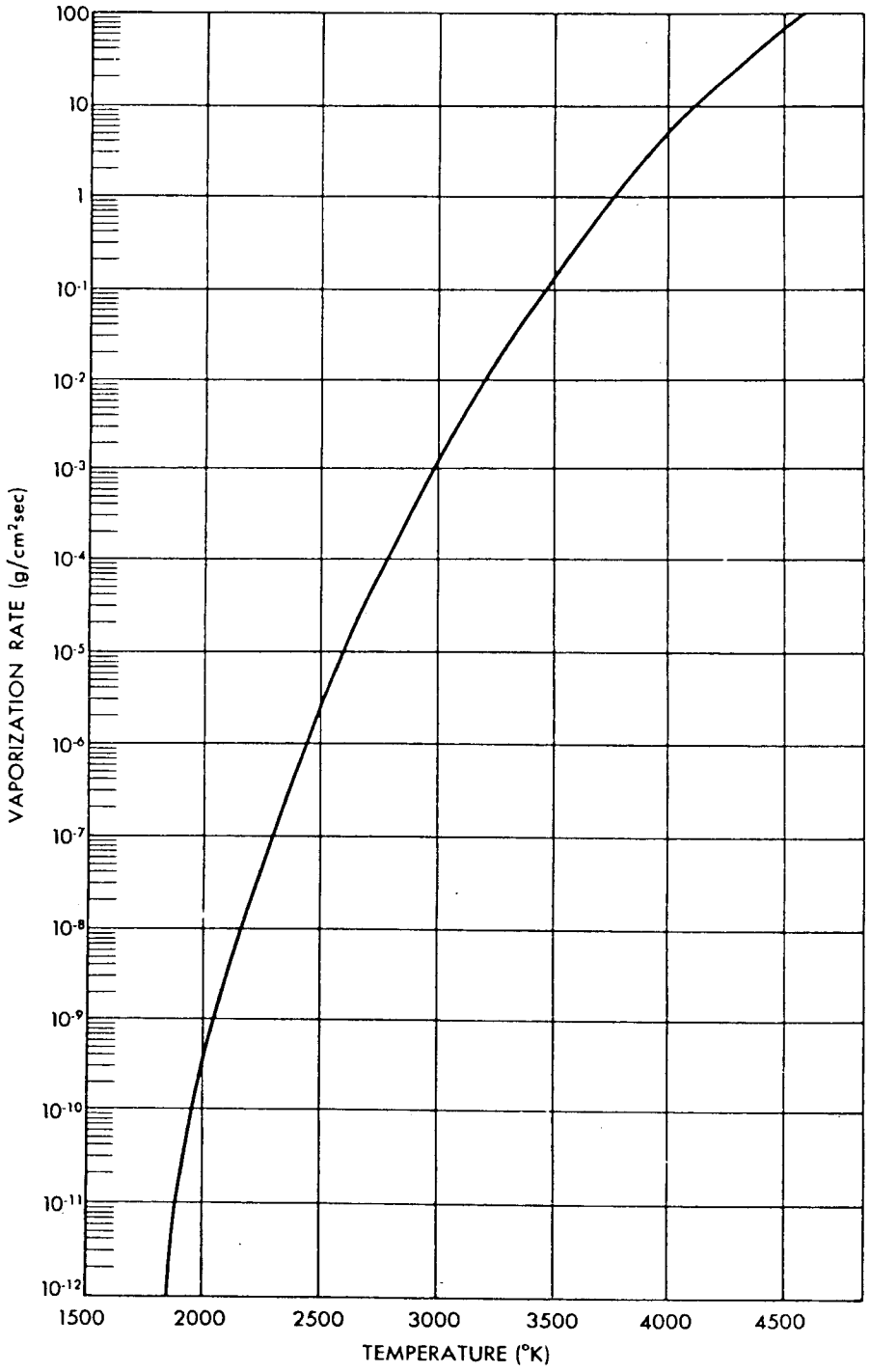

Figure 9b Free vaporization rate of graphite

Table 3b

Vapor Pressure of Graphite

Temperature		Partial Pressures of Species in Atmospheres					Equivalent Vapor	Free Vaporization
°K	°C	C	C_2	C_3	C_4	C_5	Pressure (atm)*	Rate (g/cm^2 sec)
1200	927	1.01×10^{-23}					1.17×10^{-23}	5.19×10^{-23}
1300	1027	2.81×10^{-21}		2.38×10^{-22}			3.54×10^{-21}	1.51×10^{-20}
1400	1127	3.21×10^{-19}	1.015×10^{-21}	4.37×10^{-20}			4.54×10^{-19}	1.87×10^{-18}
1500	1227	1.95×10^{-17}	1.34×10^{-19}	3.96×10^{-18}			3.16×10^{-17}	1.26×10^{-16}
1600	1327	7.08×10^{-16}	8.55×10^{-18}	2.04×10^{-16}			1.34×10^{-15}	5.15×10^{-15}
1700	1427	1.68×10^{-14}	3.34×10^{-16}	6.55×10^{-15}	3.11×10^{-20}	4.47×10^{-20}	3.72×10^{-14}	1.39×10^{-13}
1800	1527	2.81×10^{-13}	8.65×10^{-15}	1.42×10^{-13}	1.62×10^{-18}	2.33×10^{-18}	7.25×10^{-13}	2.64×10^{-12}
1900	1627	3.47×10^{-12}	1.59×10^{-13}	2.45×10^{-12}	5.52×10^{-17}	8.00×10^{-17}	1.08×10^{-11}	3.81×10^{-11}
2000	1727	3.34×10^{-11}	2.21×10^{-12}	3.10×10^{-11}	1.03×10^{-15}	1.92×10^{-15}	1.31×10^{-10}	4.61×10^{-10}
2500	2227	1.79×10^{-7}	4.30×10^{-8}	2.62×10^{-7}	2.15×10^{-10}	3.17×10^{-10}	1.05×10^{-6}	3.23×10^{-6}
3000	2727	5.43×10^{-5}	3.03×10^{-5}	1.41×10^{-4}	6.05×10^{-7}	8.97×10^{-7}	5.38×10^{-4}	1.51×10^{-3}
3500	3227	3.18×10^{-3}	3.20×10^{-3}	1.38×10^{-2}	1.68×10^{-4}	2.49×10^{-4}	5.30×10^{-2}	0.138
4000	3727	6.67×10^{-2}	0.103	0.47	1.10×10^{-2}	1.64×10^{-2}	1.83	5.29
4500	4227	0.708	1.52	7.13	0.276	0.408	28.3	65.0
5000	4727	4.66	12.9	72.5	3.54	5.20	288	627
5500	5227	21.6	72.8	839	27.8	40.6	3000	6240
6000	5727	77.6	307	6390	152	220	21600	43000

*The equivalent pressure is that pressure which would be observed if the vapor were monatomic carbon.

III. Specific Considerations for the Graphite Curtain*

A. Deployment of Curtain

The basic concept is to hang the graphite curtain in the scrape off region between the plasma and first wall. The curtain can be draped in the fashion shown schematically in Figure 1. The curtain would be attached to the first wall by alumina or magnesia pegs (Figure 10) such that no part of the graphite curtain physically touches the first wall.

The minimum separation of the curtain from the first wall is determined by the length of the low thermal conductivity stud required to maintain a reasonable temperature difference between the curtain and the first wall. As we shall see later, this thickness is less than a millimeter.

B. Material Specifications

For the basis of calculation, we have chosen to use Union Carbide T-50S carbon-graphite yarn (Reference 13). The curtain is assumed to be woven in a 2-dimensional pattern such as described in Section II.

The total area of graphite curtain that is required for a reactor like UWMAK-II[9] is $2.8 \times 10^7 cm^2$. If we assume the curtain thickness is made up of 6.6 micron diameter carbon fibers woven to a 0.2 cm thickness (uncompacted) and a 50% theoretical density, then the compacted volume of the curtain is $2.8 \times 10^7 cm^2 \times 0.2 \times 0.5 = 2.8 \times 10^6 cm^3$. The total weight of the curtain is $2.8 \times 10^6 cm^3 \times \frac{2g}{cm^3} \cong 5.6 \times 10^6$ grams. The surface area of the graphite fibers is given (Ref. 13) as $10^4 cm^2$ per gram of material so that the total surface area of the fibers in the graphite curtain is $\sim 5.6 \times 10^{10} cm^2$.

The cost of this amount of curtain material is estimated to be ~$100,000.

---

* When necessary, reactor parameters from UWMAK-II[9] will be used to represent a typical large scale fusion reactor.

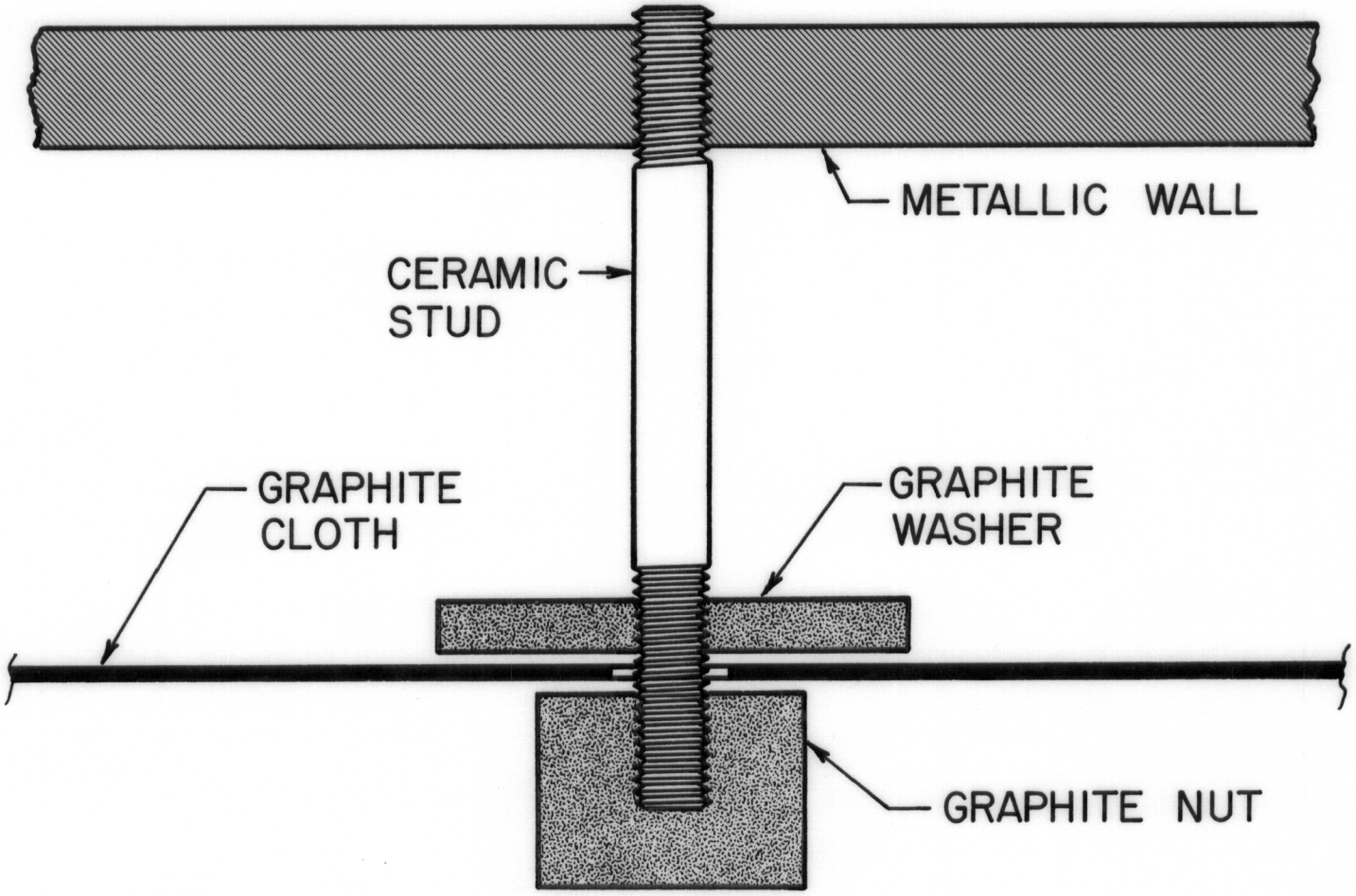

Figure 10. Possible attachment of graphite cloth to metallic first wall.

C. Vacuum Considerations

The low vapor pressure and high melting point of graphite makes it an excellent candidate for application in high vacuum environments.[14] Unfortunately, the graphite which was used in the past was extremely porous and contained considerable gas which presented noticeable outgassing loads. Because of this property and the poor fabricability of graphite, most previous workers did not consider this form of carbon as being suitable for high vacuum requirements.

Graphite is commonly thought to absorb gases readily because of experience with carbon and charcoal at high pressures and low temperatures. However, most gases adsorb only weakly on graphite and below 10^{-5} torr, gases are very reluctant to adsorb on graphite.[14]

The rapid advance in graphite technology has led to new forms of graphite and carbon-carbon composites which have demonstrated extremely good properties in high vacuums. Beitel[14] has shown that at low pressures, graphite is not as efficient a gas absorber as was commonly thought. For example, the sticking probability for molecular hydrogen on graphite is $<3 \times 10^{-6}$. Hart et al.[15] found that the maximum oxygen coverage on graphite at 300°K and 10^{-9} torr to be 0.02 monolayers.

An analysis of the vacuum properties of graphite must include the following three considerations:

1. Internal gas content
2. Adsorption
3. Vapor pressure of carbon

There is wide variation on the outgassing of graphite, mainly because there are so many types of graphite. For example, heating unbaked general purpose graphite to ~1400°C causes 300 torr-liters/g of gas (45% N_2, 45% CO, 10% CO_2) to be evolved.[16] Heating that material to 2000°C causes another

75 torr liters/g of gas (mainly CO) to be evolved. On the other hand, Nuclear Grade extruded graphite evolved only 20-80 torr-liters/g of gas (82% H_2, 17% CO, 1% N_2) up to the same temperature. Beitel[17] has investigated the gas evolution from graphites which have undergone a 24 hour, 300°C degassing procedure. The results are shown in Table 4 and it is interesting to note that the outgassing is no worse than a tungsten filament. It is important to note that gas evolution values of 5×10^{-3} to 6×10^{-2} torr-liter/g are obtained for temperatures up to 2100°C. Such gases are mostly H_2 and CO_2 and the level of evolution is only ~0.01% of general purpose, unbaked graphite.

If we use a value of 6.3×10^{-2} torr-liter per gram for the graphite curtain, we calculate that 352,800 torr-liter of gas load could be evolved in heating such baked graphite in our curtain to ~2100°C. This can be compared to the pumping capacity of a reactor like UWMAK-II which is ~2700 torr-liters/sec.

There are two factors which make the above evolved gas numbers too high and probably of little concern. First of all, one would probably degas the curtain at much higher temperatures than 300°C thus reducing the amount of gas in the cloth. Secondly, once this curtain was in place, it could be resistively heated to further evolve gases before the plasma was turned on. Once outgassed, this material would be very clean until the system was reopened and exposed to air.

In order to completely analyze the adsorption of gases on graphite, one should consider

1. activation energy for adsorption
2. sticking probability
3. heat of adsorption
4. surface coverage
5. activation of energy of surface diffusion
6. recombination coefficient

Table 4 [17]

Gas Evolution from Graphite and Tungsten[a] composition (%) H_2-CO-CO_2-HC.[b]

Temperature range	Fine grain extruded	Processed pyrolytic tape	Pyrolytic	Tungsten
600-1000 K	2-80-13-5	5-5-1-90	80-15-1-1	50-50-1-1
1000-1250 K	20-45-25-10	30-5-1-65	50-20-5-25	10-90-1-1
1250-1850 K	15-80-2-2	40-40-4-15	10-60-30-1	5-95-0-0
1850-2400 K	20-80-0-0	20-70-5-5	15-80-5-1	1-100-0-0
		Total gas evolved		
(Torr·liters/cm^2)[d]	7.5×10^{-4}	1.6×10^{-4}	8.4×10^{-5}	2.3×10^{-4}
(Torr·liters/g)	6.3×10^{-2}	2.3×10^{-2}	5.7×10^{-3}	2.0×10^{-2}

a The gas which is liberated during Joule heating of ribbon samples in vacuum after having been subjected to a 24-h, 300°C bake.

b HC represents the combined hydrocarbon fraction most of which is methane.

c High-density high-purity highly oriented pyrolytic graphite plate.

d Based upon geometric surface area.

We will not go into detail on all of these properties here and the reader is referred to reference (14) for more details. However, a few points are worth noting. Recent experiments[17] have established an upper limit of 10^{-8} for sticking of molecular hydrogen on graphite. The sticking probability of atomic hydrogen (the most likely form of graphite in a fusion reactor) has been reported as 0.015[18] and 0.038[19] at room temperature and $P < 10^{-5}$ torr. The sticking probability of CO on graphite is 5×10^{-5} and decreases rapidly as surface coverage approaches 0.01 monolayer.[17]

We can now make an estimate of the amount of gas releases if all that adsorbed on the surface was to be emitted. Assuming that there is ~0.02 monolayer of oxygen present, then if each oxygen atom occupies 10 $\mathring{A}^2$ ($10^{-15}cm^2$) we should have ~11.2×10^{23} oxygen atoms on $5.6 \times 10^{10} cm^2$ of graphite surface. This amount of oxygen represents 1.92 moles or ~32,000 torr liters of gas. Again, it is easy to visualize this gas being pumped out during pre-burn baking of the cloth.

D. Temperature Considerations

1. Equilibrium Curtain Temperatures

We will address this problem by making the following assumptions of the curtain:

. All photons and charged particles escaping from the plasma are absorbed in the first row of graphite fibers.

. The only way the curtain loses heat is by radiation to the first wall (neglect that conducted through the ceramic standoffs)

. The thickness of the curtain has no bearing on the heat transfer as long as more than one layer of filaments is present.

. Assume no nuclear heating effects (these will be on the order of a few watts/cm^3)

The basic formula for heat transfer between the curtain and the first wall is

$$q = \varepsilon_{eff}\sigma(T_c^4 - T_{FW}^4)$$

where q is the incident energy including all photons and charged particles,

ε_{eff} is the effective emissivity coefficient,

$$\varepsilon_{eff} = \left[\frac{1}{\frac{1}{\varepsilon_c} + \frac{1}{\varepsilon_{FW}} - 1}\right]$$

and ε_c is emissivity of the curtain (graphite)

ε_{FW} is the emissivity of first wall

σ is the Stephan-Boltzeman Constant

T_c is the curtain temperature

T_{FW} is the first wall temperature

The following values were used to calculate T_c

$$q_{max} = 12.4 \text{ watts/cm}^2 \text{ (UWMAK-II)}$$

$$\varepsilon_c = 1$$

$$\varepsilon_{FW} = 0.5, 0.8, 1.0$$

$$\sigma = 5.69 \times 10^{-12} \text{watts cm}^{-2} {}^\circ\text{K}^{-4}$$

$$T_{FW} = 873^\circ\text{K}$$

hence

$$T_c = \left(\frac{q}{\varepsilon_{eff}\sigma} + T_{FW}^4 \right)^{1/4}$$

For $\varepsilon_{eff} = 1.0$,

$$T_c = \left[\frac{12.4}{5.69 \times 10^{-12}} + (8.73 \times 10^2)^4 \right]^{1/4}$$

For $\varepsilon_{eff} = 1.0$ $T_c = 1288^\circ\text{K}$ (1016°C)

For $\varepsilon_{eff} = 0.8$ $T_c = 1348^\circ\text{K}$ (1075°C)

For $\varepsilon_{eff} = 0.5$ $T_c = 1491^\circ\text{K}$ (1218°C)

Hence, the curtain will run from ~1000 to 1200°C depending on the emissivity of the first wall.

2. Thickness of Ceramic Stand Off Pads Required

It is of interest to calculate the minimum thickness of stand-off pads in Figure 10 required to maintain a 400, 500 and 600°C temperature drop from the curtain to the blanket so that the first wall does not overheat (above ~600°C). We will assume that we use magnesia pads which must maintain the proposed ΔT in a distance X_{min} if the heat flow is equal to that which is incident on the magnesia pads, or,

$$q = k \frac{\Delta T}{X_{min}}$$

k for magnesia = $0.000675 \frac{\text{watts}}{\text{cm°C}}$

$q = 12.4 \frac{\text{watts}}{\text{cm}^2}$

$\Delta T = 400, 500, 600°K$

$\Delta T = 600°K$ $\qquad X_{min} = \frac{k}{q} \Delta T$

$$= \frac{6.75 \times 10^{-4} \times 600}{12.4}$$

$$= 0.033 \text{ cm (13 mils)}$$

At $\Delta T = 500°K$ $\qquad X_{min} = 0.028$ cm (11 mils)

At $\Delta T = 400°K$ $\qquad X_{min} = 0.022$ cm (9 mils)

3. Time-Temperature Behavior

In UWMAK-II, the graphite curtain will run at T_c for ~5000 seconds and then its temperature will drop during the recycle time (approximately 300-400 seconds). The heat content (above 600°C) of a square cm of graphite curtain at 1200°C is,

$$C_p \Delta T \times \left(\frac{\text{wt}}{\text{unit area}}\right) \cong \frac{0.16 \text{ cal}}{\text{gm°C}} \times 600°C \times \frac{5.6 \times 10^6 \text{g}}{2.8 \times 10^7 \text{cm}^2}$$

$$\cong 20 \text{ cal/cm}^2.$$

The initial radiation rate at 1000°C is ~3 cal/sec cm^2. Hence, after plasma shut down, it will take only a few seconds for the curtain to cool down to the first wall temperature. Likewise, it will take only a few seconds (or less) to heat up from 600°C to 1000°C.

E. Mechanical Properties

The strength requirements of the graphite curtain are minimal since it is not a structural component and need only bear its own weight. If the attachment points are at 1 meter intervals and the graphite washers and clamps engage 1 inch (or 2.54 cm) of cloth, each attachment point will support 1 m^2 of cloth (or about 1.3 kg of weight). The tensile breaking strength of graphite cloth is reported as varying between 4 and 18 kg/cm depending on the fiber. This is approximately an order of magnitude or more larger than the requirement.

F. Neutronic Effects

There have been three reactions considered here;

$C^{12}(n,\alpha)Be^{9}$ and $C^{12}(n,\alpha)He^{4}$ He^{5}

$C^{12}(n,\gamma)C^{13}$

$C^{13}(n,\gamma)C^{14}$

We have assumed that the specific gravity of the graphite is 2.0 g/cm^2 and the isotope density is;

$C^{12} = 9.889 \times 10^{22}$ cm^{-3}

$C^{13} = 1.11 \times 10^{21}$ cm^{-3}

The neutron spectrum from the first wall of UWMAK-I was assumed to apply because exact UWMAK-II spectra are not available at the present time.

Some of the calculated results are given below

. Helium production rate is ~0.97×10^{13} atoms/cm^3-sec

or 9.7×10^{-5} appm/sec

3.4×10^{-1} appm/hr

8.38 appm/day

3059 appm/year

6118 appm/2 years (~0.6%)

. Build up of ^{14}C after 2 years of irradiation is as follows (see Figure 12 also)

1.02×10^{5} dps/cm^{3} of graphite

2.9×10^{11} dps in total curtain

7.7 curies of activity total.

. Build up of afterheat at t = 0 in ^{14}C in 2 years is as follows

7.7×10^{-16} MW/cc

2.2×10^{-9} MW (2.2 milliwatt) Total

There is very little afterheat to worry about.

. The decay of the radioactivity after 2 years is as follows

7.7 curies at t = 0

7.7 curies after 2 years

7.5 curies after 200 years

6.2 curies after 2000 years

In other words, the C^{14} half life (5,600 years) is so long that we effectively do not get rid of the activity in a time considered reasonable for above ground storage. It should be pointed out that the impurities in carbon will essentially dominate the total radioactivity of the curtain.

Figure 12 - Buildup of Radioactivity, Afterheat and Helium in Graphite Curtain

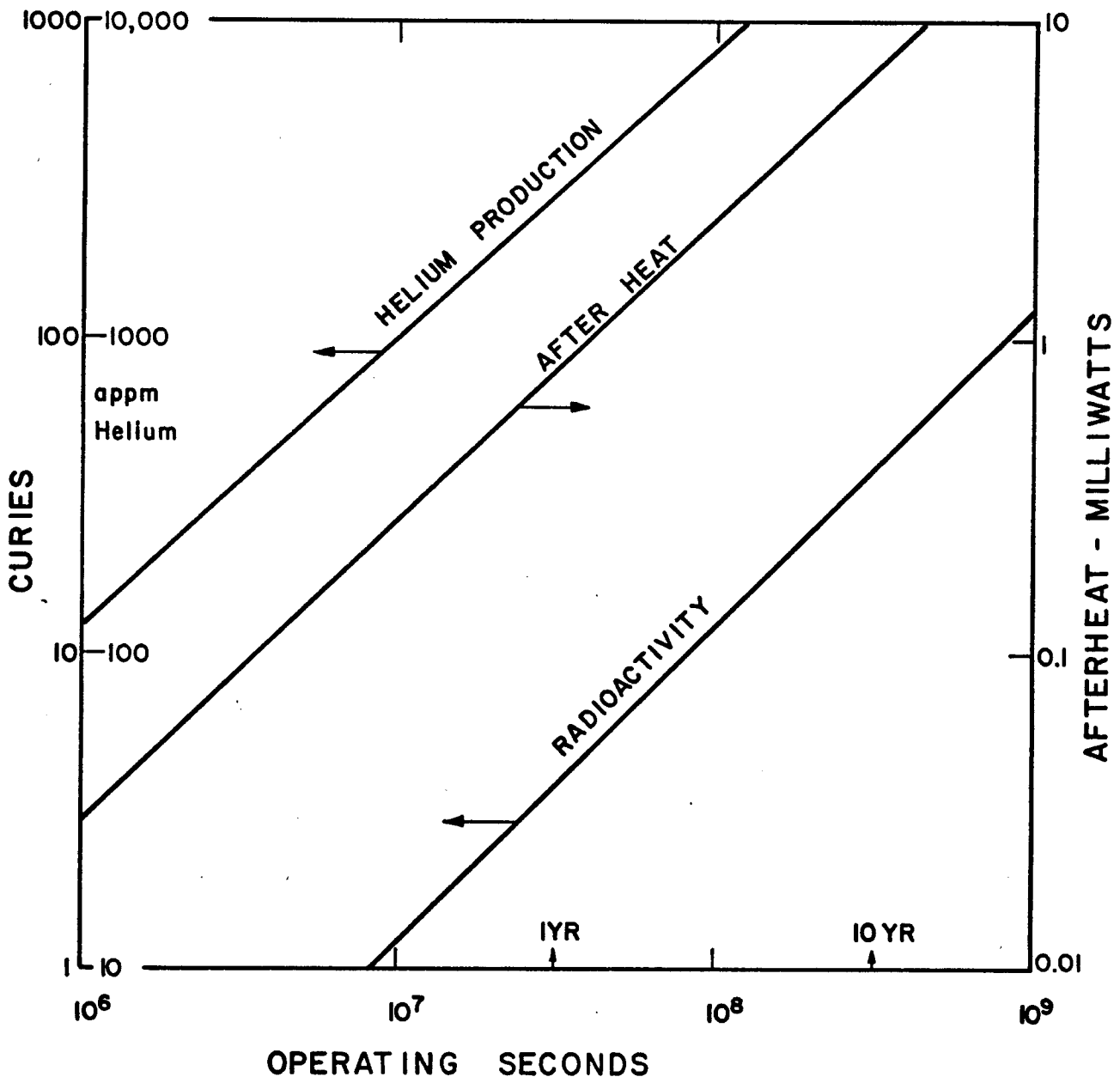

G. Displacement Damage and Swelling

In order to calculate the amount of swelling in graphite at 1000-1200°C, we must compare the damage in the curtain to that obtained in a fission reactor where all the swelling data has been established. One way in which this can be accomplished is to compare damage on the basis of the total number of atoms displaced in either a fission or fusion reactor spectrum and assume that the damage is only dependent on the total number of displacements. The dpa crossection for graphite has been calculated by Gray and Morgan[20] and it has been modified to fit into a 46 group neutron structure consistent with the neutron spectra. See Table 5.

It is calculated that the dpa rate corresponding the UWMAK-I conditions is

1.73×10^{-7} dpa/sec

1.5×10^{-2} dpa/day

5.5 dpa/year

Using the dpa rate of 5.9×10^{-22} dpa/fission spectrum neutron[21] one finds that the CTR dpa rate is equivalent to a fission spectrum flux of $\sim 2.9 \times 10^{14}$ n/cm^2/sec.

One can get an idea of the potential dimensional changes to be expected from the irradiated graphite by scanning figure 13. This figure displays the swelling as a function of dpa level, temperature, and the degree of anisotropy of the graphite. It appears that the largest effects will be found in anisotropic graphite which is most similar to the form in typical graphite cloth. Lesser effects are seen

Table 5

Data Used in Calculation of Displacement Damage in Graphite

Group No.	Upper Energy (eV)	Flux (n/cm 4 sec) at UWMAK-I First Wall	Displacement Cross section-barns
1	1.4918 (+7)*	1.02213 (+14)	270.4
2	1.3499 (+7)	5.71820 (+12)	297.5
3	1.2214 (+7)	3.80135 (+12)	313.6
4	1.1052 (+7)	5.48941 (+12)	266.2
5	1.0000 (+7)	4.69964 (+12)	247.5
6	9.0484 (+6)	3.82653 (+12)	254.8
7	8.1873 (+6)	3.11143 (+12)	486.4
8	7.4082 (+6)	2.69767 (+12)	285.6
9	6.7032 (+6)	2.42107 (+12)	348.7
10	6.0653 (+6)	2.32419 (+12)	345.7
11	5.4881 (+6)	2.22100 (+12)	418.1
12	4.9659 (+6)	2.21289 (+12)	503.6
13	4.4933 (+6)	2.26542 (+12)	643.6
14	4.0657 (+6)	2.42901 (+12)	746.1
15	3.6788 (+6)	2.63525 (+12)	844.8
16	3.3287 (+6)	2.90263 (+12)	655.7
17	3.0119 (+6)	3.29001 (+12)	708.7
18	2.7253 (+6)	3.81248 (+12)	525.2
19	2.4660 (+6)	1.32089 (+13)	533.1
20	1.8268 (+6)	1.57116 (+13)	556.0
21	1.3534 (+6)	1.68548 (+13)	606.5
22	1.0026 (+6)	1.81145 (+13)	641.5
23	7.4274 (+5)	2.12012 (+13)	655.7
24	5.5023 (+5)	2.04969 (+13)	648.3
25	4.0762 (+5)	1.60409 (+13)	618.7
26	3.0197 (+5)	5.70661 (+12)	564.8
27	2.2371 (+5)	1.92206 (+13)	498.7
28	1.6573 (+5)	2.56284 (+13)	427.9
29	1.2277 (+5)	4.10730 (+13)	336.5
30	6.7379 (+4)	3.14386 (+13)	197.3
31	3.1828 (+4)	2.34361 (+13)	101.6
32	1.5034 (+4)	1.77938 (+13)	50.9
33	7.1017 (+3)	1.40619 (+13)	25.3
34	3.3546 (+3)	9.08034 (+12)	12.6
35	1.5846 (+3)	4.84094 (+12)	6.2
36	7.4852 (+2)	2.37074 (+12)	3.0
37	3.5358 (+2)	9.61259 (+11)	0.8
38	1.6702 (+2)	3.11505 (+11)	0
39	7.8893 (+1)	7.87407 (+10)	0
40	3.7267 (+1)	1.53249 (+10)	0
41	1.7603 (+1)	2.29795 (+ 9)	0
42	8.3153 (+0)	2.68982 (+ 8)	0
43	3.9279 (+0)	2.52431 (+ 7)	0
44	1.8554 (+0)	2.00425 (+ 6)	0
45	8.7643 (-1)	1.62317 (+ 5)	0
46	4.1399 (-1)	1.58639 (+ 4)	0

* (+7) refers to 10^7

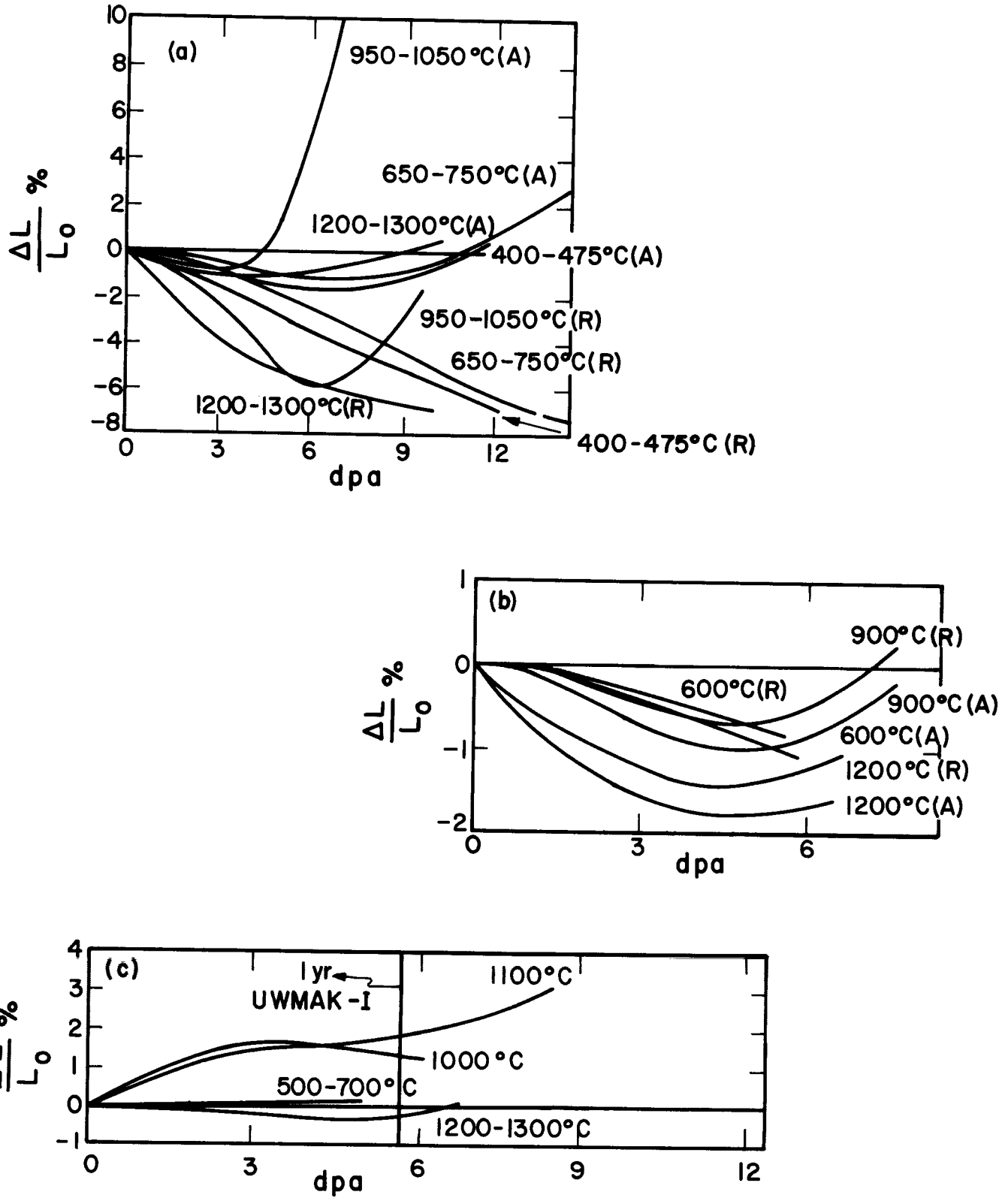

Figure 13 - Summary of Dimensional Changes of (a) anisotropic, (b) near isotropic (c) isotropic graphites. See G. B. Engle and W. P. Eatherly, High Temperatures - High Pressures, Vol. 4, 119-158, (1972) for complete referencing of data.
A = axial direction
R = radial direction

in near-isotropic and isotropic materials.

Figure 13 shows that after ~1 year of CTR irradiation at ~1200°C, the axial dimensions might shrink ~1% and the radial dimensions by ~6%. The overall density reduction is ~4%. After 2 years of irradiation, the axial dimensions may actually expand by 1-2% where the radial dimensions may have contracted to 7-8% of their original value.

Much less of an effect is found in near or strongly isotropic graphite. From Figure 13b we see that both the radial and axial dimensions might have contracted by 1-2%. It is not certain where the crossover point to expansion is but indications are that this might occur close to 2 years of irradiation.

Figure 13c shows that high density fine grained isotropic graphites are the most damage resistant. Less than 0.5% contraction is expected after 1 year of CTR operation but indications are that cross over will occur shorlty after one year and one may be into a "run away" expansion stage before 2 years of CTR exposure has been completed.

Recently, Peggs and Mills[21,22] have reported on radiation damage to thornel 50S at relatively low damage levels (3×10^{-4} to 0.47 dpa) and relatively low temperatures (420-600°C). It was found that the crystalline size did not change by more than ±25% from 40 Å. The "c" axis spacing at 420°C varied as shown below

dpa	C-Å	% change
0	6.85	-
3×10^{-4}	6.80	-0.73
0.12	6.74	-1.6
0.47	6.92	+1.0

In summary, the most logical form of the graphite material for CTR curtains will be quite anisotropic. Such material probably will contract during irradiation. There appears to be no "run away" swelling problem for anisotropic graphite as long as the curtain does not experience more than two years of CTR exposure. There may be "run away" expansion problems for near isotropic and isotropic materials after ~11 dpa (2 years CTR exposure) at ~1200°C.

H.) Sputtering of Graphite Curtain

The side of the curtain facing the plasma in a UWMAK-II type of reactor will be subjected to the following high energy charged particle fluxes (assuming a 90% efficient divertor)

- 20 keV* D ions, $1.3 \times 10^{14} cm^{-2} s^{-1}$
- 20 keV T ions, $1.3 \times 10^{14} cm^{-2} s^{-1}$
- 20 keV He ions, $6.0 \times 10^{12} cm^{-2} s^{-1}$
- 20-3500 keV unthermalized He ions, (Mean energy ~100 keV) $2.2 \times 10^{11} cm^{-2} s^{-1}$
- 10-14 MeV neutrons, $1.66 \times 10^{13} cm^{-2} s^{-1}$
- 0 -10 MeV neutrons $3.91 \times 10^{14} cm^{-2} s^{-1}$

All of these particles will cause carbon atoms to be sputtered from the first wall. These sputtered (probably neutral) atoms will diffuse into the plasma, absorb energy and become ionized, and finally diffuse out of the plasma to re-bombard the graphite curtain. The flux of sputtered atoms from the first wall can be calculated by

$$\phi = \sum_i S_i (E) \phi_i (E)$$

where S_i (E) is the sputtering ratio (atoms/particle) for the i th particle with energy E on carbon.

ϕ_i (E) is the flux of particles at energy E incident on the carbon surface.

It is very difficult to locate experimental values of S_i for carbon, especially at the energies typical of fusion devices. We summarize in table 6 and in figures 14-16 what information is available. No information

* mean energy = 3/2 T_i

Table 6

Summary of Data on Sputtering of Carbon

Ion	Energy keV	S Atom/particle	Reference
H,D,T,	———	———	———
He	0.4	0.06	23
He	0.5	0.07	24
C	45	~0.4	25a
Ne	0.4	0.01	23
Ar	24	~2.5	26
K	0.5	0.13	24
Kr	45	2.4	25b
Xe	0.5	0.17	24
Cs	10	1.97	24
Hg	0.5	0.16	23
n	———	———	———

on hydrogen isotopes was found and only low energy data on He bombardment is available.

It is well known that the qualitative variation of sputtering coefficient with bombarding particle energy is as shown for silver in Figure 14. The peak of the curve occurs roughly at the energy where a transition between hard sphere and weakly screened Coulomb interactions takes place. This energy, E_A, is defined roughly as

$$E_A \cong 2E_R Z_1 Z_2 (Z_1^{2/3} + Z_2^{2/3})^{1/2} \frac{M_1 + M_2}{M_2}$$

where E_R is the Rydberg energy (13.61 eV)

M_1, M_2 are the atomic weights of the projectile and target atoms respectively

Z_1, Z_2 and the atomic numbers of the projectile and target atom respectfully.

A summary of E_A values for various materials is shown in Table 7.

Table 7

Summary of E_A values for Surface Bombardment

	E_A - KeV			
Projectile	C	V	Fe	Mo
H	0.37	1.9	2.7	4.2
D	0.40	2.0	2.8	4.3
T	0.43	2.2	3.2	4.9
He	0.96	4.2	6.1	8.9
C	5.0			

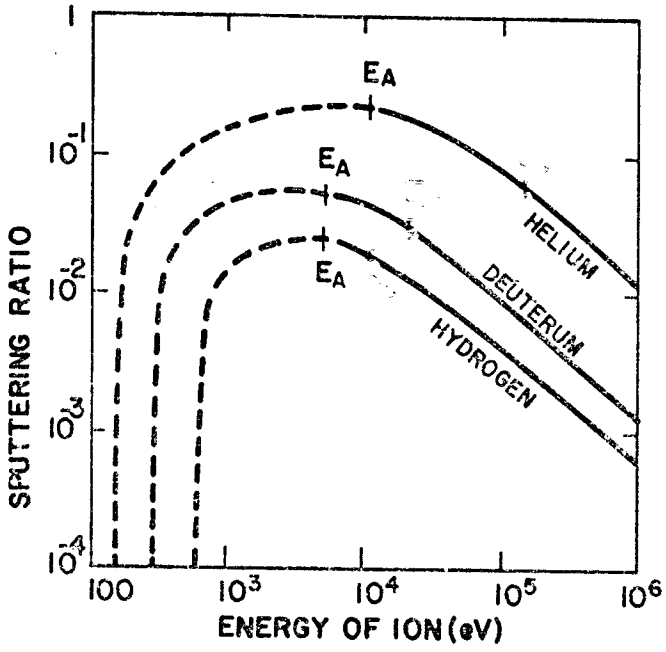

Figure 14 Calculated sputtering ratio of various ions on silver, as a function of energy. The energy limits for hard sphere collision is E_A. The dashed portion of the curves indicate regions of decreased reliability. (R. S. Pease, Rendiconti SI.F. Corso 13:158, Sept. 1959)

The first point to note is that the E_A value for He on carbon is within a factor of 2 of the energy for which sputtering data is available. Hence, since figure 14 is on a log-log basis we can assume that the sputtering values in table 6 are maximum values for helium on carbon. Furthermore we will assume that the value for 45 keV C on C of ~0.4 [25a] is characteristic of fusion reactor bombardment because it is within a factor of 2 from the mean bombarding energy. However, we will use $S_c \tilde{=} 0.6$ for 20 keV carbon on carbon in order not to under-estimate the self ion sputtering.

It is obvious that 20 keV helium atoms are much above the peak in the curve of figure 14 and hence the sputtering ratios should be <0.07. It is difficult to know how much less, but Behrisch[36] has found that S~0.06 for 4 keV helium on carbon. Hence, we will use 0.06 as a maximum sputtering coefficient.

Since no data is available for the sputtering value of deuterium or tritium on graphite, we will estimate it from the ratio of (S_{He}/S_D) typical of bombardment of metals. Some characteristic values are given below for 20 KeV atoms.

Element	S_{He}/S_D Calculated[26]	Exp[27a, 27b]
V	9	-
Nb	9.2 - 9.8	12 (at 1100°C)
Mo	9.1 - 9.8	-
Cu	9 - 9.2	-

Hence, it appears that if we estimate the sputtering ratio for D&T is a factor of ~10 lower than that for helium on graphite, then $S_{D,T}$ 0.006.

The atomic sputtering ratio for neutrons on graphite is again unknown but we might estimate it relative to other metals. Figure 16 shows such data and if we extrapolate if for carbon, we find that S_n is on the order of 1/2 that for neutrons on gold. The sputtering ratio for Au has recently been found to vary from $<6.4 \times 10^{-4}$ by Keller[28], $\sim 3 \times 10^{-4}$ by Behrisch[29] to 3×10^{-3} by Garber et al.[30]

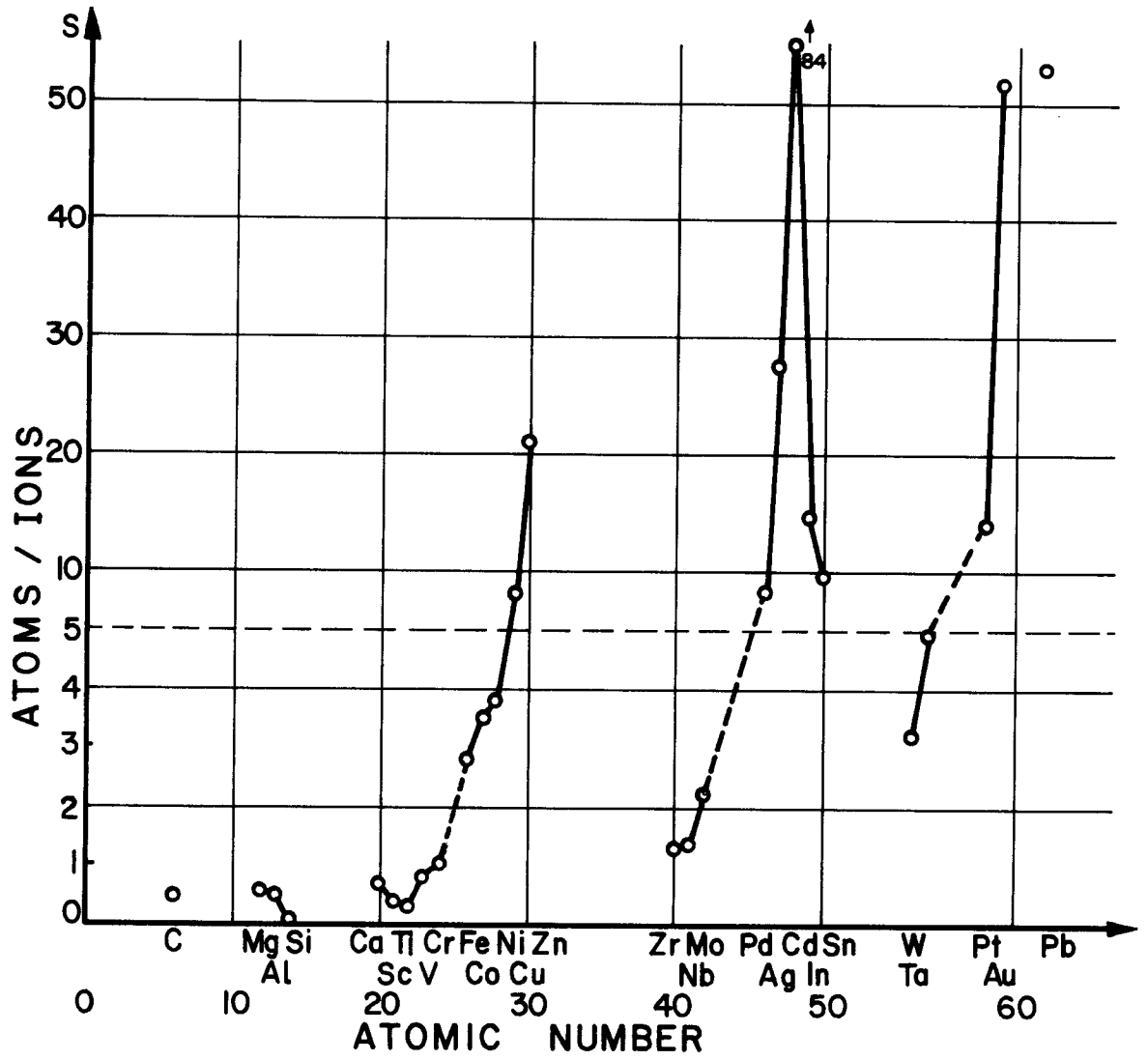

Fig. 15 Selfsputtering ratios for some materials at 45 keV ion energy.[25a]

Figure 16

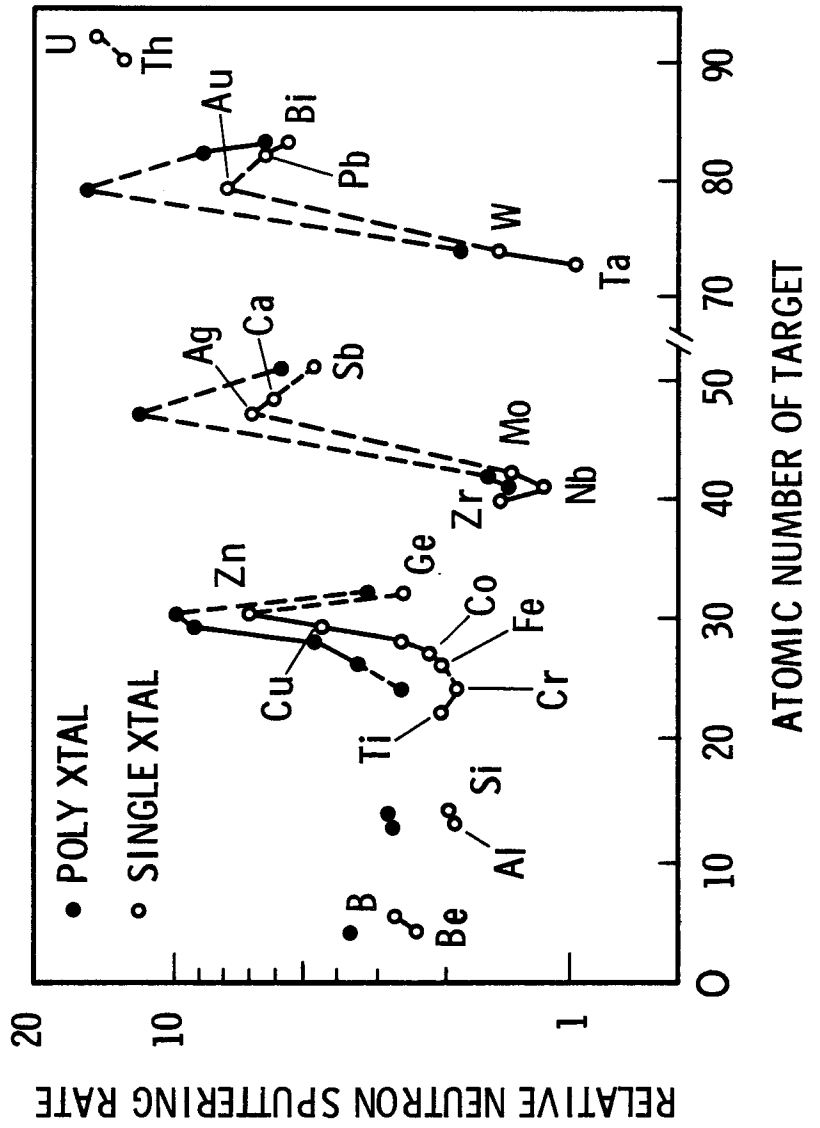
PERIODIC VARIATION OF
NEUTRON SPUTTERING RATE — GARBER et. al. (30)
POLY XTAL
SINGLE XTAL
RELATIVE NEUTRON SPUTTERING RATE
ATOMIC NUMBER OF TARGET
20
10
1
0
10
20
30
40
50
70
80
90
U
Th
Au
Bi
Pb
W
Ta
Ag
Ca
Sb
Mo
Nb
Zr
Zn
Ge
Co
Fe
Cr
Cu
Ti
Si
Al
B
Be

So that not to bias our case, we will again choose a very pessimistic value of $S_n = 1.5 \times 10^{-3}$ for carbon. When better data is available we will adjust our calculations

We are now in a position to calculate the flux of sputtered atoms from the graphite curtain.

$$\begin{aligned}\phi &= 2 \times 1.8 \times 10^{14} \times 0.006 \\ &+ 6.0 \times 10^{12} \times 0.06 \\ &+ 2.2 \times 10^{11} \times 0.02 \\ &+ 5.57 \times 10^{14} \times 0.0015 \\ &= 3.4 \times 10^{12} \text{ atoms/cm}^2\text{/sec}\end{aligned}$$

The above calculations show that the flux of sputtered atoms is influenced by neutron bombardment (~25%) and that even if one did not have a divertor, the total sputtering rate would be about seven times that with a 90% efficient divertor.

At this point, one should estimate the extra effect of self sputtering via carbon atoms returning to the graphite wall with energies of ~20-30 keV. If the reactor has a 90% efficient divertor and if the sputtering ratio for carbon on carbon is ~0.6, then the total carbon flux back to the curtain is $\sim 3.4 \times 10^{11}$ cm^{-2}sec^{-1} and, effectively, 40% of those will stick in the graphite fibers. The self ion contribution to the sputtered atom flux is then ~6% of the initial carbon flux from the surface. For the purposes of further calculations, we will assume the equilibrium flux to the plasma is approximately

$$3.6 \times 10^{12} \text{ carbon atoms/cm}^2\text{/sec (90\% efficient divertor)}$$

and the effective wall erosion rate is due to a flux of

$$\phi_{eff} = 3.4 \times 10^{12} \text{carbon atoms cm}^{-2}\text{sec}^{-1}$$

when the carbon sticking coefficient is taken into account. The erosion rate is then,

$$\begin{aligned}d(t) &= \phi_{eff} \frac{t \, A_w}{N_o \, \rho} \\ &= 3.4 \times 10^{12} \times \frac{12}{6 \times 10^{23} \times 2} \times t \\ &= 3.4 \times 10^{-11} \frac{\text{cm}}{\text{sec}} \times t\end{aligned}$$

The amount of wall removed as a function of time is

2.9×10^{-2} microns/day

11 microns/year

21 microns/2 years

Hence, if the filaments are on the order of 6 microns thick, then approximately the first 4 filaments will be eroded in a two year time span.

The total mass of carbon removed in 2 years is then ~130kg. This carbon will most likely end up in the vacuum pumping system (e.g., liquid Li films on UWMAK-I in the pumps themselves) or replated on the reactor walls.

I. Effect on Tritium Inventory

There are two main ways that a graphite blanket might tend to accumulate tritium.

1. adsorption on the graphite surface
2. implantation into the graphite fibers.

Again, very little information exists on the adsorption of molecular or atomic hydrogen on graphite at pressures of $<10^{-5}$torr and 1200°C. As stated previously, the sticking probability of atomic hydrogen (the most likely form in a fusion reactor) is between 0.015 and 0.038 at pressures of $<10^{-5}$ torr and temperatures of 300°K. This will probably be reduced as the temperature is raised, but let us assume a pessimistic value of 0.04.

Since the surface area of the graphite filaments is 2.8×10^{10}cm^2, and the average surface density of atoms is $(8.03 \times 10^{22}\text{atoms/cm}^2)^{2/3} = 1.9 \times 10^{15}\text{atoms/cm}^2$, there is a potential of 5.32×10^{25} possible sticking sites. If the sticking coefficient is 0.04 then $\sim 2.1 \times 10^{24}$ atoms could stick. This is 3.52 mole which would be evenly divided between deuterium and tritium. Hence,

1.76 mole of tritium, (5.3g) is the most that could possibly be adsorbed on the surface. This would amount to ~50,000 curies or about 10^{-2}% of the total plant inventory.

In order to consider the implanted tritium we must know the range of the incoming particle, and the diffusivity of tritium after it has been implanted. The range of H,D and tritium has been plotted in Figure 17 for energies of 0-80 keV.[31] It can be seen that at 24 keV the range of tritium is ~8000 Å.

The time taken for the tritium to diffuse out of the graphite depends on whether the tritium diffuses through the matrix or out through microcracks in the graphite. If the tritium diffuses through the matrix, the average concentration in the graphite can then be simply calculated by

$$\text{(average concentration)} \cong \frac{1}{3} \frac{\text{(generation rate)(path length)}^2}{\text{Diffusivity}}$$

$$\cong \frac{1}{3} \frac{(\phi/R) \times (R^2)}{D}$$

$$C_{ave} = \frac{1}{3} \frac{\phi R}{D}$$

Since $\phi = 1.3 \times 10^{14}$ tritium atoms $cm^{-2} sec^{-1}$

$R = 8 \times 10^{-5}$ cm

then $C = \frac{3.5 \times 10^9}{D}$ atoms/cm^3 or $C = \frac{49 \times 10^9}{D}$ atoms/cm^3 if $R = \frac{1}{2}$ fiber/thickness

There is only one known study on the diffusivity of tritium in carbon

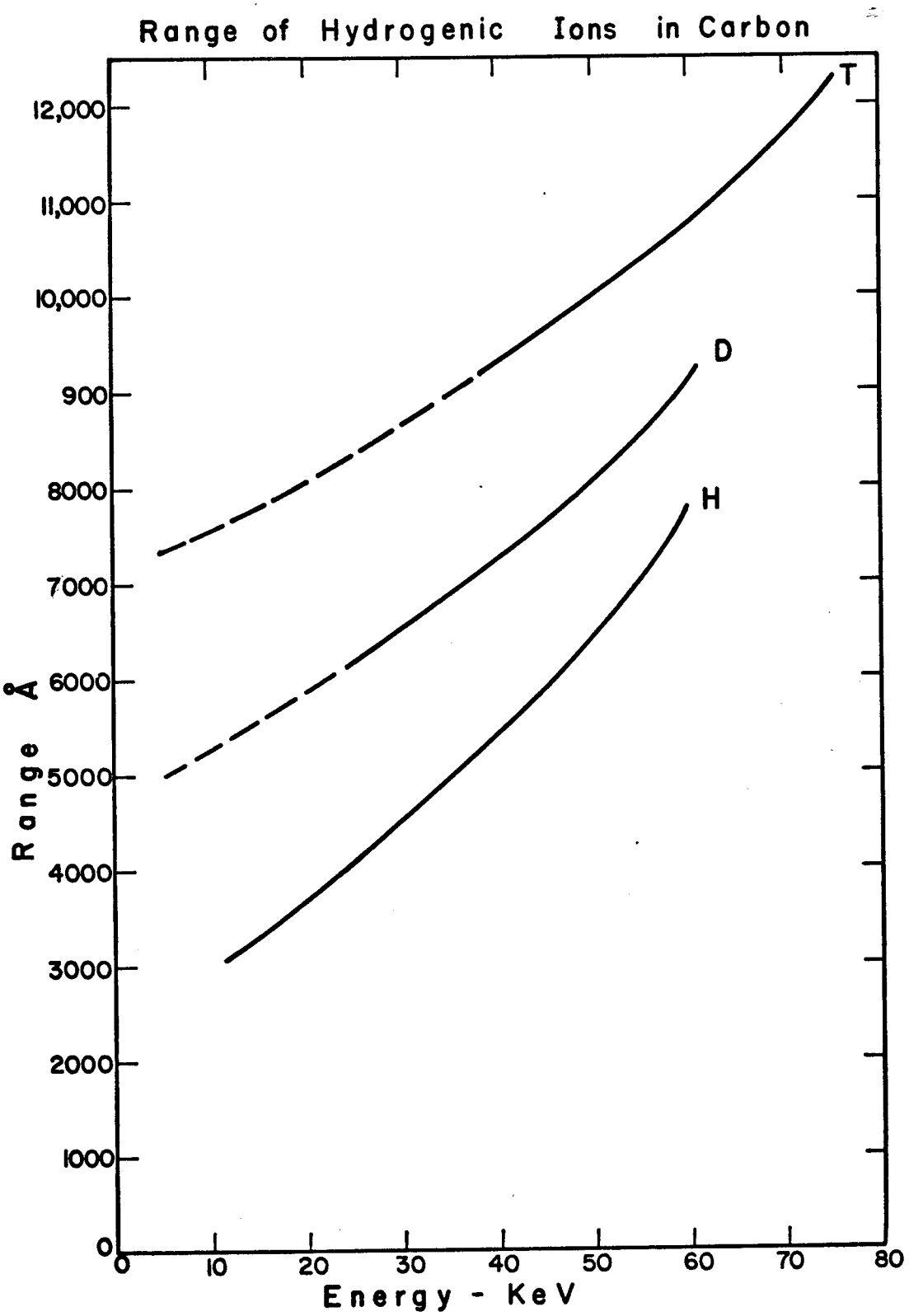
Range of Hydrogenic Ions in Carbon
T
D
H
12,000
11,000
10,000
900
8000
7000
6000
5000
4000
3000
2000
1000
0
Range Å
0
10
20
30
40
50
60
70
80
Energy - KeV

Figure 17

We were unable to obtain release of the information on tritium diffusion at the time of publication.

at 1200°C activity =11,400curies

From the above calculation, it does not appear that the curtain will have any impact on the tritium inventory due to implantation even if a very low diffusivity is assumed.

J.) Compatibility

One concern that needs to be investigated is the possibility that some chemical reactions will take place between the graphite and the hydrogenic atoms in the vacuum chamber. This reaction could take place during the burn, ($p<10^{-5}$ torr) as well as inbetween burns when the "ash" is flushed out and the hydrogen pressure is raised to $\sim 10^{-2}$ torr.

The most probable reaction that could take place is the following

$$C + 2D_2 \rightleftarrows CD_4$$

$$C + 2T_2 \rightleftarrows CT_4$$

The temperature and pressure dependence of this reaction (in the absence of radiation) is shown in Figure 18. Above 400°C at P $\sim 10^{-5}$ atm or

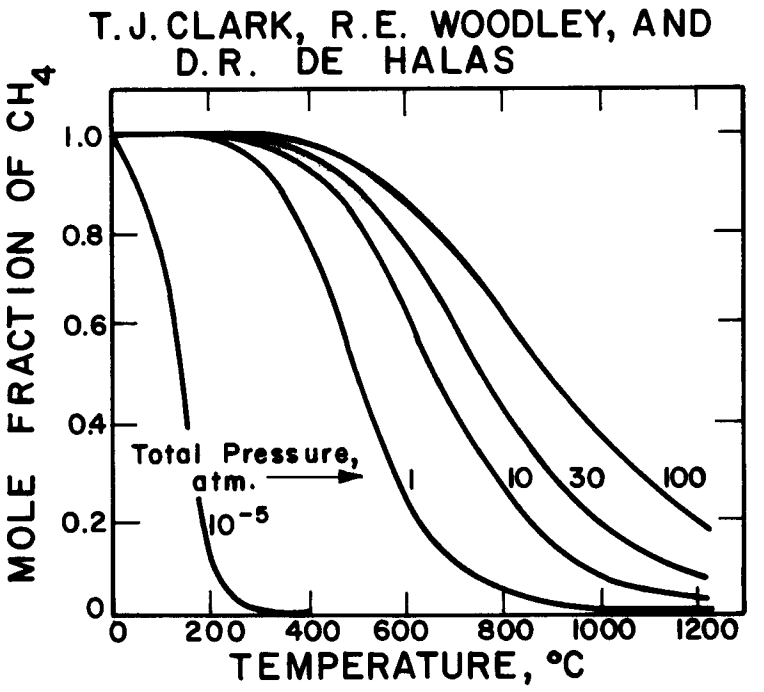

Fig. 18 The mole fraction of methane formed at equilibrium for the hydrogen-graphite reaction.[32b]

10^{-2} torr, the amount of "methane" formed is negligible. Since the curtain will probably operate at ~1000-1200°C at 10^{-5} torr and cool down to the first wall temperature of 600°C between burns, we can see that the worst case is when the pressure is raised to ~10^{-2} torr.

A pessimistic assessment can be made of the magnitude of this potential reaction if we assume that ~1% of the carbon in the chamber will form methane between burns. This also assumes that the flush times (~100 seconds) are large enough to establish equilibrium. The number of moles of hydrogen isotopes in the UWMAK-I chamber at 10^{-2} torr is

$$\text{Moles of D,T} = \frac{\text{(volume of chamber-liters)}}{22.4} \times \frac{10^{-2}}{760}$$

$$= 4.55$$

Hence, ~0.023 moles of carbon could be consumed per complete burn cycle. The number of burns in UWMAK-I per year is ~5000 (100% plant factor) which implies 115 moles of carbon (~1.4 kg) will be consumed per year. This is about 0.03% of the total blanket per year. The actual amount would be expected to be much less than this under realistic circumstances. It is also interesting to note that this would amount to a uniform erosion rate of ~0.004 micron/year which on the plasma side of the curtain, is less than 0.1% of the wall erosion due to sputtering.

A note of caution should be raised here as it is known that radiation has a pronounced effect on the reaction of graphite with hydrogen. No quantitative data exists at this time and such data would be expected to be very dependent on material.

K.) Electrical Effects

The resistivity of graphite and other CTR metals is given below as a function of temperature

	Micro-ohm - cm			
Material	RT	500°C	1000°C	1500°C
graphite	3500	2700	2100	1600
316 SS	30	105	130	
Mo	6	16	26	

Hence, the resistivity of the graphite is still one to two orders of magnitude above that of normal CTR structural metals so that eddy current losses should be considerably less in the curtain than in the wall.

L.) Miscellaneous

It is of interest to calculate the range of 0-3.5 MeV helium particles in graphite in order to estimate the zone of heat generation. The range versus energy curves are shown in Figure 19.

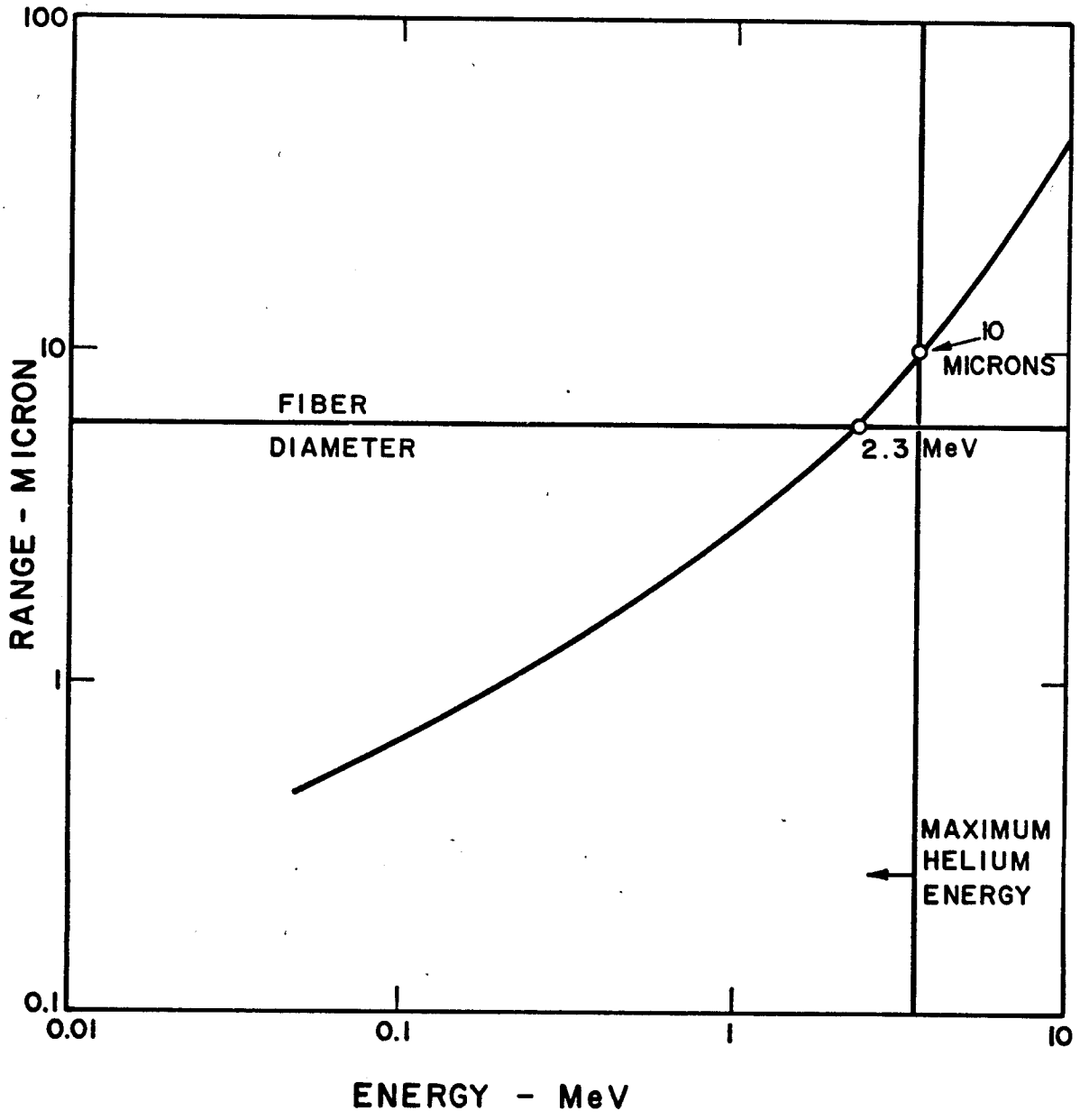

Figure 19 - Range of He^4 in Carbon

IV. Plasma Effects

A. High Z vs Low Z Impurities-Impact on Plasma Energy Balance

We indicated in the introduction some of the detrimental effects of high Z impurities on plasma behavior. From an energy balance viewpoint, high Z impurities greatly enhance radiative losses from a steady state plasma. This increase is mainly due to increased line and recombination radiation which dominates when high Z materials are present even at electron temperatures of 10 keV. The severity of the problem is shown by calculating radiative losses from plasmas with high Z versus low Z impurities.

Radiative losses in a steady state plasma is approximately given for a single impurity by[33]

$$P_{RAD} = P_x \left(1 + \frac{.0379\ \xi Z_{im}^{\ 4}}{Z_{eff} T_e} + \frac{8.6 \times 10^{-4} \xi Z_{im}^{\ 6}}{Z_{eff} T_e^{\ 2}} \right)$$

where

$$P_x = 4.8 \times 10^{-31}\ n_e^{\ 2} Z_{eff}\ T_e^{\ 1/2} \quad (\text{watts/cm}^3)$$

and

$$Z_{eff} = \frac{1}{n_e} (n_i + Z_{im}^{\ 2}\ n_{im}).$$

Here P_x is the power radiated via bremsstrahlung, the second term in brackets is the ratio of line radiation to bremsstrahlung, and the third term is the ratio of recombination radiation to bremsstrahlung. ξ_{im} is the ratio of impurity density (n_{im}) to the electron density (n_e), Z_{im} is the atomic number of the impurity, T_e is the electron temperature in keV and n_i is the ion density. At 10 keV and $n_e = 10^{14}/\text{cm}^3$, Mo will have at least 3 electrons remaining[3] so that the formula of Hinnov is applicable. He gives $P_{RAD} \simeq 2\ \xi\ n_e^2 \times 10^{-26} \text{w/cm}^3$ which, for 1% Mo and $n_e = 10^{14}\text{cm}^{-3}$, gives $P_{RAD} = 2\ \text{w/cm}^3$. By contrast, under the same plasma conditions, 1% carbon impurity

gives P_{RAD} (Z = 6) = 0.02 watts/cm^3. The ratio, P_{RAD} (Z = 6; 1%) to P_{RAD} (Z = 42; 1%) is 10^{-2}. This gives a clear indication of the improvement in the energy balance when low Z impurities are present. In addition to this, another benefit comes from the fact that low Z impurities require fewer electrons to maintain charge neutrality. Thus, for a given electron density, 1% Mo means $\frac{n_{DT}}{n_e}$ = 0.58 whereas 1% C yields $\frac{n_{DT}}{n_e}$ = .94. Since the power output is directly proportional to n_{DT}^2, the same percentage of a low Z impurity allows for higher deuterium and tritium densities, and therefore higher power output. As a consequence, the alpha power that heats the plasma is greater and this, together with the decreased radiative losses, makes igniting a plasma easier.

B. Impact in Tokamaks

A quantitative measure of the impact of impurities on tokamak plasma performance is shown in Figures 20 and 21. These results are based on a calculational model previously developed which includes alpha heating, radiative losses, and thermal losses due to conduction-convection.[5] The plasma energy containment time is based on the trapped ion mode[34] which yields pessimistically short confinement times in high temperature plasmas and thus conservative predictions. As can be seen from Figure 20, impurity levels of less than 0.1% iron cause the plasma current required to achieve ignition to more than double. Furthermore, relatively modest impurity concentrations, such as 0.3 to 0.5%, cause the plasma current required for ignition to increase beyond 10 MA.

By contrast, the impact of carbon impurities at levels up to 5% is not as severe as the high Z results. Figure 21 shows the effect of varying concentrations of C on the plasma current required for ignition. The sharp increase in plasma current beginning at about 6% carbon is due to the decrease in the ion density when the total electron density is held fixed.

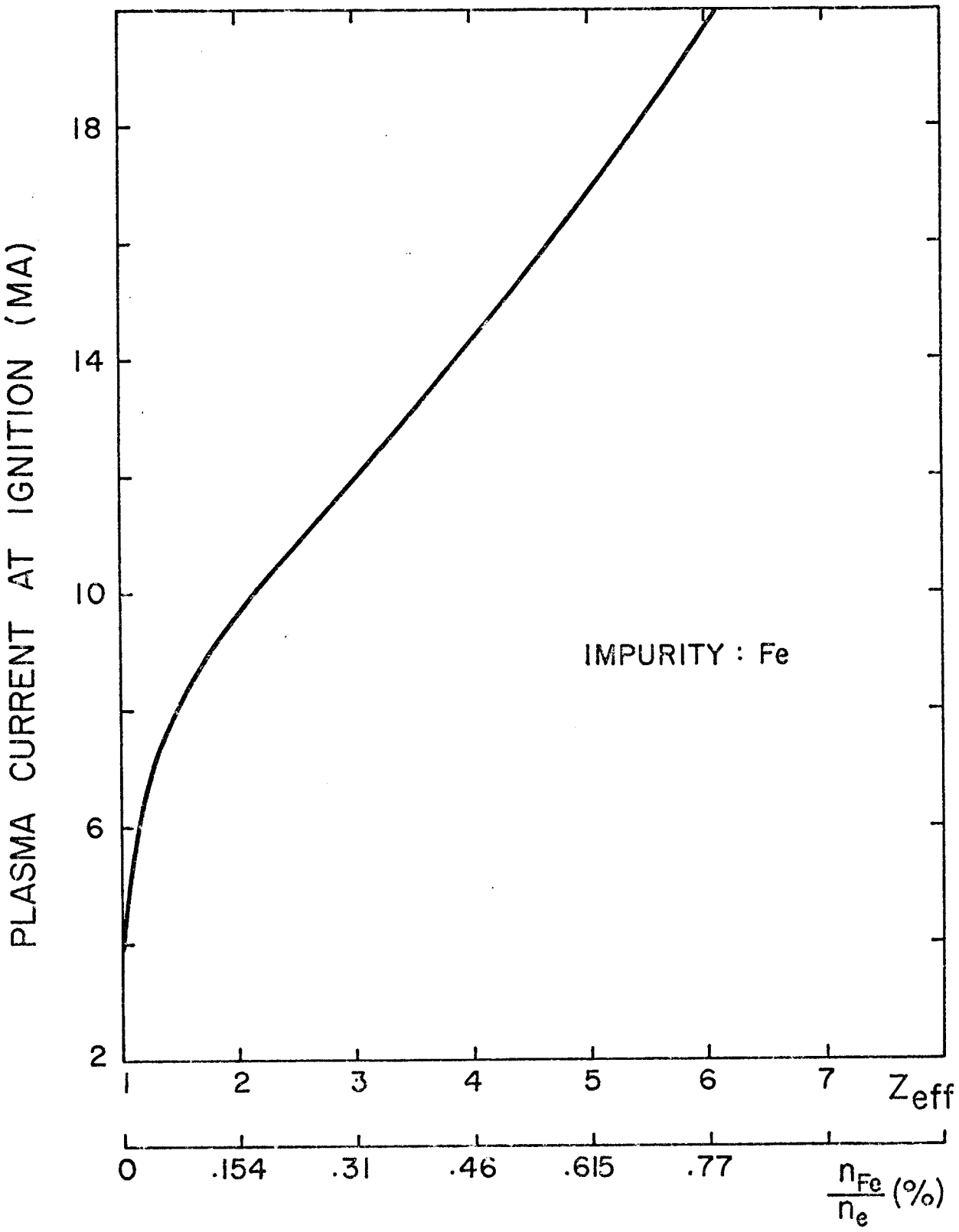

Figure 20 - Plasma Current at Ignition as a Function of the Amount of Impurity in the Plasma.

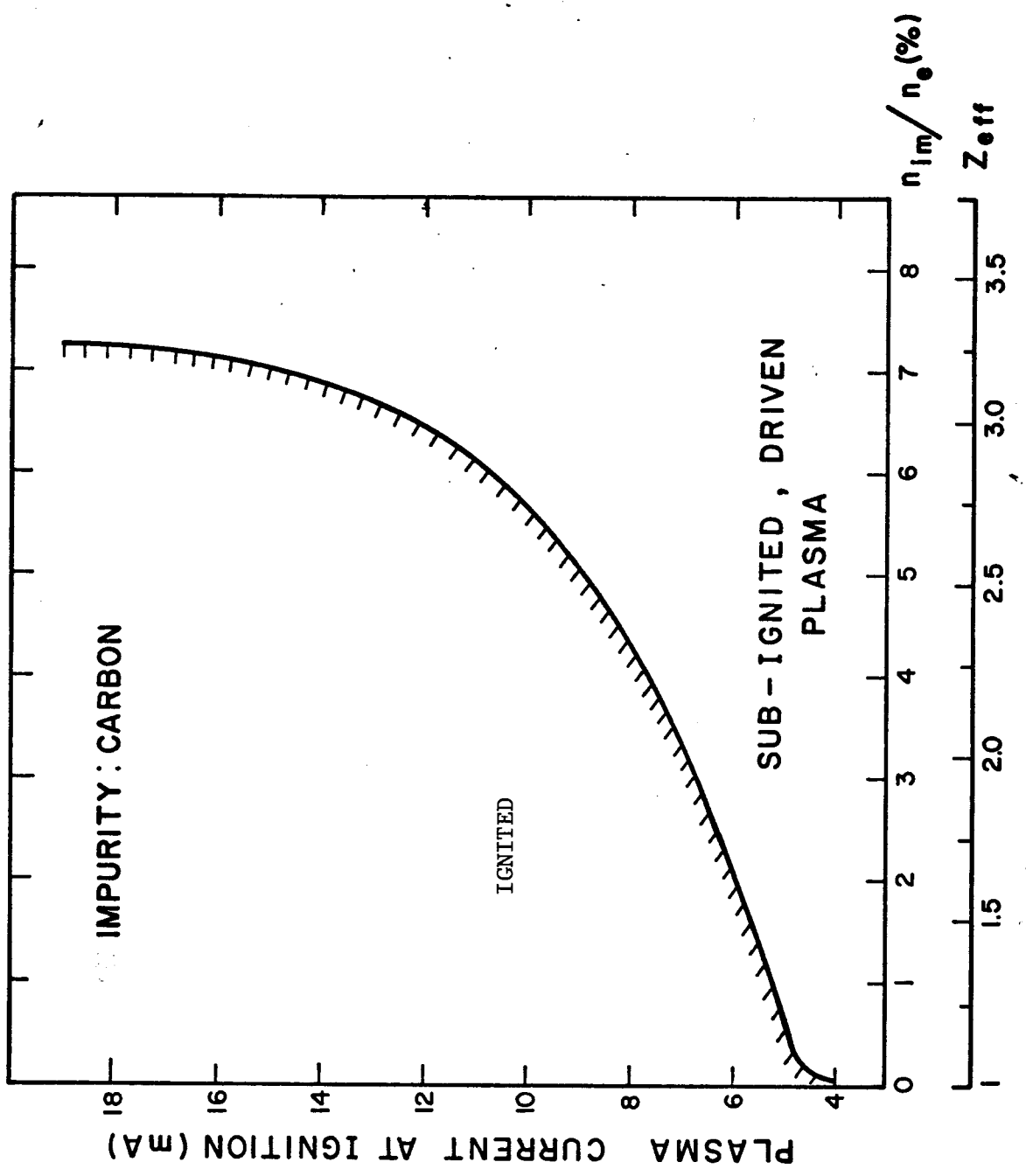
PLASMA CURRENT AT IGNITION (mA)
18
16
14
12
10
8
6
4
IMPURITY: CARBON
IGNITED
SUB-IGNITED, DRIVEN PLASMA
0
1
2
3
4
5
6
7
8
n_{im}/n_e(%)
1
1.5
2.0
2.5
3.0
3.5
Z_{eff}

Figure 21

The power produced by a typical reactor grade DT fusion plasma in a Tokamak is shown in Figure 22. The plasma parameters are comparable to those of the UWMAK-II conceptual design[9] and we have assumed 21.5 MeV per fusion event. One notes that the power level decreases almost linearly up to carbon concentrations of 6.5%. For higher impurity levels, the drop in power becomes more severe. Systems with impurities greater than about 7% are unignited and require external power input to maintain the plasma in energy equilibria. Such driven plasma reactors have been discussed previously.[5]

C. Estimated Impurity Levels on a Plasma

An important question relative to impurity levels in the plasma is the expected impurity level under steady state conditions. A simple model will help give some indication of the answer to this. Consider a tokamak plasma system which may have a divertor. There are three main components of this system important to the problem at hand. These are shown schematically in Figure 23. Let n_{DT} be the plasma DT density, n_{He} be the helium density, $\tilde{n}_{He}$ be the nonthermal helium density, and n_{imp} be the impurity density. These each have characteristic confinement times, τ_{DT}, τ_{He}, $\tau_{\tilde{He}}$, and τ_{imp}. The corresponding sputtering coefficients are denoted by S_{DT}, S_{He} and $S_{\tilde{He}}$. Let S_{imp} be the self sputtering coefficient and let S_n be the neutron sputtering coefficient. We define η as the fraction of ions diffusing from the plasma which strike the first wall.

δ is defined as the fraction of particles coming off the wall which reach the plasma and is sometimes referred to as the shielding capacity of the divertor. The factor $(1-\eta)\cdot(1-\delta)$, is the overall divertor efficiency. From a simple mass balance across the interface between the plasma and the scrape-off layer, one can derive the following expression for the equilibrium concentration of impurities:

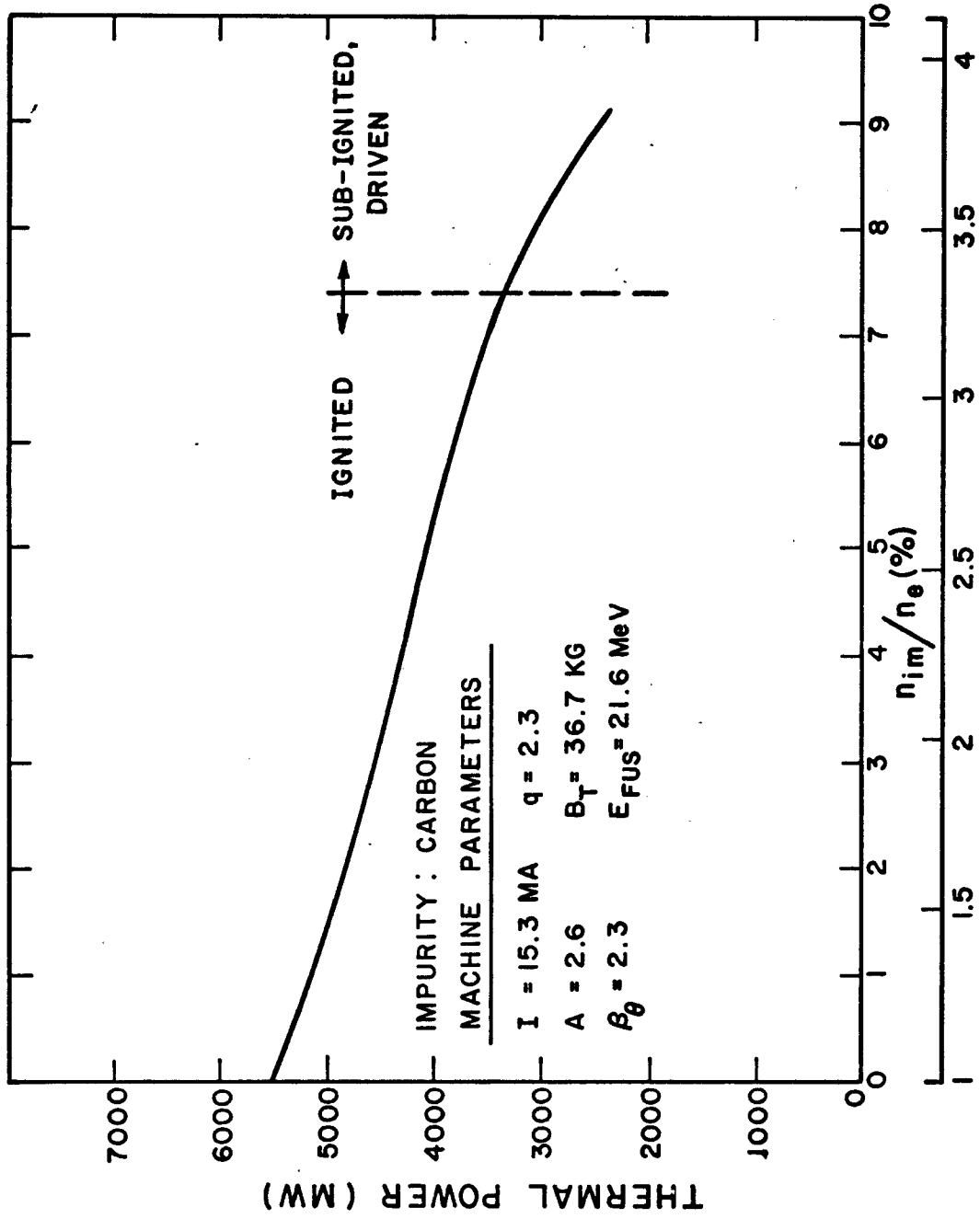
THERMAL POWER (MW)
7000
6000
5000
4000
3000
2000
1000
0
IGNITED
SUB-IGNITED, DRIVEN
IMPURITY : CARBON
MACHINE PARAMETERS
I = 15.3 MA q = 2.3
A = 2.6 B_T = 36.7 KG
β_θ = 2.3 E_{FUS} = 21.6 MeV
n_{im}/n_e(%)
1
1.5
2
2.5
3
3.5
4
5
Z_{eff}
0
1
2
3
4
5
6
7
8
9
10

Figure 22

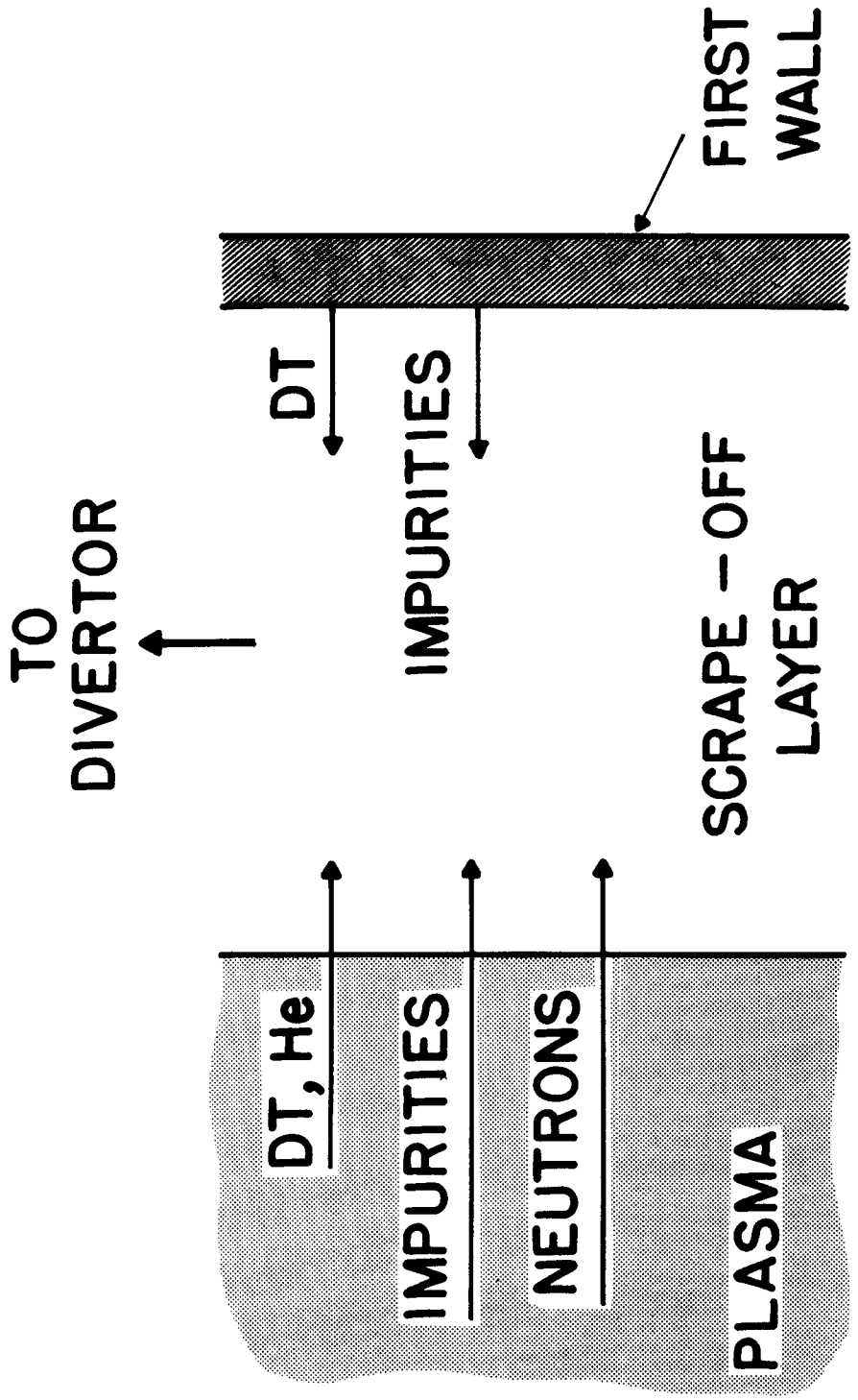

Figure 23 - Schematic used for equilibrium impurity levels in CTR plasmas

$$n_{imp} = \frac{\eta\delta\left(\frac{n_{DT}}{\tau_{DT}} S_{DT} + \frac{n_{He}}{\tau_{He}} S_{He} + \frac{\tilde{n}_{He}}{\tau_{\tilde{He}}} \tilde{S}_{He}\right)\tau_{imp}}{(1 - \eta\delta\, S_{imp})}$$

$$+ \frac{\delta A_w}{V_p} \frac{S_n \phi_n \tau_{imp}}{(1 - \eta\delta\, S_{imp})} \quad .$$

Here, ϕ_n is the neutron flux at the first wall, V_p is the plasma volume, A_w is the first wall area, and $\eta\delta\, S_{imp}$ has been assumed to be less than one. For $\eta\delta\, S_{imp}$ greater than one, the impurity level continues to build without reaching an equilibrium.

For sample calculations, we will use a set of plasma parameters which characterize a conceptual tokamak power reactor such as UWMAK-II. The parameters pertinant to this discussion are listed in Table 8. Note that these calculations are based on $Z_{eff} = 1$. Thus, the calculations of impurity concentrations and the ratio $\frac{n_{imp}}{n_e}$ are accurate for this ratio less than about 1-5% carbon. Above this level, one must self consistently evaluate n_e including the higher impurity concentrations. We therefore restrict our quantitative conclusions to cases where $\frac{n_{imp}}{n_e} \lesssim .05$. We estimate particle fluxes to the first wall from $(\frac{n}{\tau}\frac{V_p}{A_w})$ and use the neutron fluxes obtained from detailed neutronics calculations for the UWMAK-II design.[9] They are also given in Table 8.

As discussed in section II-H, the sputtering values for charged particles and neutrons are not well known. We have therefore considered three sets of sputtering coefficients; high values, low values, and a set of "most likely" values as given in Table 9. The largest variations occur in the neutron sputtering coefficient. The high value is based on the "chunk emission" phenomenon reported by Kaminsky et.al.[35] while the low and most likely values characterize atomistic sputtering. The high and most likely values of

D and T sputtering on carbon are based on recent results of Behrisch.[36]

The expected impurity concentration was calculated from the formula for n_{imp} using these sputtering coefficients and the plasma parameters and neutron fluxes in Table 8. The results are summarized in Table 10 for three cases corresponding to no divertor, a moderately good divertor (η = .1, δ = .9), and an excellent one-way divertor (η = 0, δ = .9). We have expressed the impurity confinement time as a multiple of the D-T confinement time by

$$\tau_{imp} = M\,\tau_{DT}$$

and presented the results as multiples of M.

These results suggest that it may be possible to operate a tokamak without a divertor if M is about 1. This may be the case if turbulent diffusion tends to carry all species from the plasma at the same rate. If the high sputtering values prevail, a divertor is essential. With a moderately good divertor (η=.1, δ=.9), M values of about 5 may be tolerable even with the high sputtering data. With the low or most likely data sets, one could tolerate M multiples of 50 to 100. Finally, if the divertor is very efficient at collecting particles diffusing from the plasma ($\eta \sim 0$) but does not shield effectively, M values of the order of 10^2 to 10^3 could be tolerated with the low and most likely data sets. If a divertor were also effective at shielding ($\delta < .1$), then M multiples greater than 10 could be tolerated even with the highest sputtering values that may occur.

We would conclude from these simple calculations that it may be feasible to operate with a carbon curtain and no divertor if $M \sim 1$ and that a moderately good divertor can most likely allow operation at acceptable levels of carbon impurity even if the impurity containment time is 10 to 10^3 times the ion confinement time.

Table 8

Parameters Characterizing a Conceptual Tokamak Fusion Reactor Plasma

$n_D = 3.23 \times 10^{13}$ cm^{-3}
$n_T = 3.23 \times 10^{13}$ cm^{-3}
$n_\alpha = 0.091 \times 10^{13}$ cm^{-3}
$n_e = 6.64 \times 10^{13}$ cm^{-3}

$T_{D,T} = 13.5$ keV
$T_e = 15.2$ keV

Confinement Time, $\tau = 4$ sec.
Assumption, $\tau_D = \tau_T = \tau_{He}$

Plasma Current = 14.9 MA
Toroidal Field Strength (on axis) = 35.7 kΓ

$\beta_\theta = 2.3$
$q = 2.3$
Plasma radius = 500 cm
Major radius = 1300 cm
Minimum wall radius = 550 cm
Plasma volume = 6.4×10^9 cm^3
Chamber wall area = 2.82×10^7 cm^2

Neutron Flux Characteristics-

14 MeV neutron wall loading (maximum) = 1.16 MW/m^2
Neutron flux at first wall ($E_n > 10$ MeV) = 1.66×10^{14} n/cm^2-sec
Neutron flux at first wall ($E_n < 10$ MeV) = 3.91×10^{14} n/cm^2-sec
Total neutron flux at first wall = 5.57×10^{14} n/cm^2-sec

Table 9

Assumed Sputtering Coefficients

	High	Low	Most Likely
S_D	.015	.001	.01
S_T	.0225	.0015	.015
S_{He}	.2	.12	.15
S_{c-c}	.8	.4	.6
S_n	.2	.0001	.0015

Table 10

CARBON TO ELECTRON DENSITY RATIOS

(PERCENT)

$[\tau_{imp} = M\,\tau_{D,T}]$

	High Sputtering Data	Low Sputtering Data	Most Likely Sputtering Data
No Divertor	M x 9.3%	M x 1.1%	M x 3.6%
$\eta = .1$ $\delta = .9$	M x 1%	M x .06%	M x 0.16%
$\eta = 0$ $\delta = .9$	M x .8%	M x .001%	M x 0.02%

D. Other Plasma Effects

In addition to the impact of impurities on the plasma energy balance, impurities also affect other aspects of plasma behavior. In the first place, impurities increase the collisionality of the plasma and this in turn effects plasma resistivity and transport. For example, the Spitzer resistivity of a plasma increases with the parameter, Z_{eff}, defined as

$$Z_{eff} = \frac{\sum_i n_i Z_i^2}{n_e}$$

The sum extends over all ionic species. A given amount of high Z impurity yields a larger Z_{eff}, and thus an increased resistivity, compared to low Z materials. For example, 1% Mo in a DT plasma yields a Z_{eff} of 18.2 whereas 1% carbon gives a Z_{eff} of 1.3. This has a direct impact on the core flux swing required to maintain the plasma current during a burn time and, in turn, on the energy storage requirements.

The effective collision frequency also varies as Z_{eff} and this impacts on collisional transport and on transport via collective processes. An example would be the collisional stabilization of plasma waves at higher Z_{eff}. The trapped ion mode growth rate decreases with increasing Z_{eff} and the mode may be stabilized above some critical concentration of impurities.

In present day toakamks, such as the ST machine at Princeton, it appears that the chamber walls and the limiter contribute about equally to the impurity content of the plasma. Typically, impurity levels of Mo (the limiter material) and the constituents of stainless steel (the chamber material) are about $10^{10} - 10^{11}$ cm^{-3} compared with an electron density of about $3 \times 10^{13} cm^{-3}$. The carbon curtain proposed here would eliminate wall initiated high Z impurities

but have little or no effect on impurities coming from the limiter. This situation can perhaps be corrected in several ways. First, the limiter can be constructed of carbon or silicon carbide rods. Complete sputtering information is not available on these materials but a silicon carbide limiter has been employed on the Doublet II experiment without any deleterious impact on plasma behavior. These experiments were not complete and the results are only tentative. However, the design of Doublet III does call for silicon carbide limiters, and other work indicates such limiters may be feasible. Our earlier studies[5] showed that silicon, as with carbon, will be fully stripped under reactor grade plasma conditions and thus not prove to be any special problem.

An alternate approach is to replace the mechanical limiter with a magnetic limiter, such as has been proposed on tokamaks which contain divertors. In such cases, of course, the problem of limiter originated impurities does not occur.

Conclusions

It has been shown that the inclusion of a carbon curtain between a D-T plasma and the first structural wall can effectively protect the first wall from charged particle erosion and protect the plasma from deleterious effects of impurity ions. The carbon cloth concept is compatible with the D-T environment, it is cheap and easily replaceable, and it may even reduce the need for divertors on Tokamak reactors.

The concept is even more applicable to near term devices (low neutron producing systems) in that the major problem with the curtain may prove to be the neutron damage induced by extended exposure to 14 MeV neutrons. The use of a carbon curtain in these devices, along with a suitable low Z limiter, will allow experimenters to study plasmas which contain less harmful, low Z impurities.

Achnowledgement

The authors would like to acknowledge partial support for this work from the United States Atomic Energy Commission and the Wisconsin Electric Utility Research Foundation.

References

1. Proceedings on a Conference on "First Wall Surface Problems for D-T Tokamak Reactors," to be published as a special issue of J. Nucl. Mat., (1974).

2. S. O. Dean et.al., Status and Objectives of Tokamak Systems for Fusion Research, WASH-1295, (1974).

3. R. F. Post, J. Nucl. Energy, Part C - Plasma Physics, 3,,233,(1961).

4. D. Meade, "Effects of High Z Impurities on the Ignition and Lawson Conditions for a Thermonuclear Reactor," MATT-989, Princeton Plasma Physics Lab., June 1973.

5. R. W. Conn, W. A. Houlberg, H. Kesner, "Parametric Studies of Driven Tokamaks, UWFDM-106, University of Wisconsin, June 1974.

6. S. K. Das and M. Kaminsky, J. Applied Phys., 44, 25 (1973), see also M. Kaminsky and S. K. Das, Appl. Phy. Letters, 21, 443 (1972).

7. G. R. Hopkins, p. 437 in the Proc. 1st Topical Meeting on the Tech. of Controlled Nulcear Fusion, ed. G. R. Hopkins, USAEC, CONF-740402-P2, 1974.

8. Wisconsin Tokamak Reactor Design, UWFDM-68, November 1973.

9. UWMAK-II, A Helium Cooled Fusion Reactor, To be published.

10. A. Fourdeaux, R. Perret, W. Ruland, General Structural Features of Carbon Fibers, Int. Conf. on Carbon Fibers, The Plastic Institute, London 1971.

11. C. W. LeMaistre, R. J. Diefendorf, The Effect of Thermal Expansion Anisotrophy on the Strength of Carbon Fibers, Tenth Biannual Conf. on Carbon, Summary of Papers, June 27-July 2, 1971.

12. Union Carbide, Industrial Graphite Engineering Handbook, (1970).

13. Union Carbide, Technical Bulletins, 465, 217, 465218, 465207.

14. G. A. Beitel, J. Vac. Sci. and Technol., 8, 647 (1971).

15. P. J. Hart, F. J. Vastola, and P. L. Walker, Jr., Carbon, 5, 363 (1967).

16. C. L. Mantell, Carbon and Graphite Handbook (Interscience, New York, 1968)

17. G. A. Beitel, Tech. Rep. NASA CR-111829 (1971).

18. R. K. Gould, Ph.D. Thesis, University of Wisconsin, Madison, Wisconsin, 1969.

19. G. A. Beitel, J. Vac. Sci. Technol. 6, 224, (1969).

20. W. J. Gray and W. C. Morgan, "Projection of Graphite Behavior in the University of Wisconsin Tokamak (Austin Design), To be Published.

21. W. C. Morgan, To be Published.

22. I. D. Peggs and R. W. Mills, Paper Number 119 in Ref. 11.

23. N. Laegreid and G. K. Werner, J. Applied Phys. 32, 365, (1961) and D. Rosenburg and G. K. Wehner, J. Appl. Phys. 33, 1842 (1962).

24. G. Carter and J. S. Colligon, Ion Bombardment of Solids, American Elsevier Publishing Comp. N. Y., 1968, p. 323, p. 325.

25a. O. Almén and G. Bruce, Nucl. Inst. and Methods, 11, 279, (1961).

25b. O. Almén and G. Bruce, Trans. 8th. Natl Vac. Symp. Wash, 1 245, (1961).

26. G. Betz, R. Dobrozemsky, F. P. Viehbock, and H. Wotke, p. 90 in Phenomena in Ionized Gases, A Conference held in Bucharest, Romania, 1969.

27a. D. Goldman and A. Simon, Phys. Rev. III, 383 1958.

27b. A. Summers, N. Freeman and N. Daly, Proc. Nucl Fusion Reactors, Conf., Culham Laboratory, p. 347, September 1969.

28. K. Keller, Plasma Phys, 10, 195 (1968)

29. R. Behrisch, R. Gahler and J. Kalus, To be Published J. Nucl Materials.

30. R. J. Barber, G. P. Dolya, V. M. Kolyada, A. A. Molden, and A. I. Federenko, JETP Lett. 7, 296 (1968).

31. L. C. Northcliffe and R. F. Schilling, Nuclear Data, 7, No. 3-4, June 1970.

32b. Nuclear Graphite, R. E. Nightingale, ed., Academic Press, New York, 1962.

33. G. Hopkins "Impurity Radiation Loss Mechanism from Fusion Reactor Plasmas," GGA-12374, Gulf Gen. At. Comp., October 1972.

34. B. B. Kadomstev and O. P. Pougste, Nucl. Fusion 11, 67, (1971).

35. M. Kaminsky and S. K. Das, "Particle Release from Niobium Under 14-MeV Neutron Impact" P.37 in Fifth Symposium on Engineering Problems of Fusion Research, Princeton University, Nov. (1973), IEEE Pub. No. 73CH0843-3-NPS.

36. R. Behrisch (personal communication) note, these results are preliminary and may vary by a factor of 2-3 when statistically sufficient data is accumulated.